Sex and Regional Differences in L-type Calcium Current Distribution in Adult Rabbit Right Ventricle: Influence Action Potential Duration and the Propensity for Cardiac Arrhythmia

by

Cassandra Marie Doinoff

Submitted in Partial Fulfillment of the Requirements

for the Degree of

Masters of Science

in the

Biological Sciences

Program

YOUNGSTOWN STATE UNIVERSITY

July, 2010

FORMAT FOR SIGNATURE AND RELEASE PAGE

Sex and Regional Differences in L-type Calcium Current Distribution in Adult Rabbit Right Ventricle: Influence Action Potential Duration and the Propensity for Cardiac Arrhythmia

Cassandra Marie Doinoff

I hereby release this thesis to the public. I understand that this thesis will be made available from the OhioLINK ETD Center and the Maag Library Circulation Desk for public access. I also authorize the University or other individuals to make copies of this thesis as needed for scholarly research.

Signature:

Cassandra Doinoff, Student Date

Approvals:

Dr. Carl Sims, Thesis Advisor Date

Dr. Mark Womble, Theis Co-Advisor Date

Dr. Jill Tall, Committee Member Date

Dr. Jozsi Jalics, Committee Member Date

Peter J. Kasvinsky, Dean of School of Graduate Studies and Research Date

ABSTRACT

Long QT syndrome (LQTS) is a form of heart disease that is known to affect 1 in 10,000 individuals (Vincent 2002). Individuals who suffer from congenital or acquired forms of LQTS are at an increased risk to develop deadly arrhythmias. Women are known to have longer rate corrected QT intervals (QTc) and action potential durations (APDs) than men, resulting in an increased risk for arrhythmia. Previous studies have indicated that this is primarily due to sex differences in the levels of the delayed and inward rectifier potassium currents, I_{Kr} and I_{Ks}, which regulate cardiac repolarization. However, recent data suggesting a role for calcium currents has lead us to re-examine the factors are responsible for sensitivity to arrhythmia generation.

The L-type calcium current ($I_{Ca\text{-}L}$) is a significant contributor to the magnitude and duration of the cardiac action potential. Recently, several reports have linked sex differences in $I_{Ca\text{-}L}$ to gender-associated arrhythmia vulnerability. In the present study, differences in the apex to base distribution of $I_{Ca\text{-}L}$ in adult male and female right ventricles were assessed by the patch clamp technique and a modified Luo-Rudy action potential model. Female base myocytes exhibited a 84.6% higher $I_{Ca\text{-}L}$ density than male base myocytes, but apex myocytes from males and females showed similar $I_{Ca\text{-}L}$ densities. Within the female right ventricle, base myocytes had a 56.5% higher current density than did apex myocytes. No differences were found between male base and apex myocytes. The increased current density observed in female base myocytes was not associated with alterations of $I_{Ca\text{-}L}$ activation or deactivation voltage characteristics. Cardiac action potential modeling indicated that increased $I_{Ca\text{-}L}$ could contribute to arrhythmia development. The data thus support the hypothesis that higher L-type calcium current densities may contribute to the propensity for arrhythmias in some individuals.

TABLE OF CONTENTS

CHAPTERS

LIST OF TABLES AND FIGURES

LIST OF ABBREVIATIONS

1. **APD** Action Potential Duration
2. **AP** Action Potential
3. **DAD** Delayed Afterdepolarization
4. **EAD** Early Afterdepolarization
5. **fSR** Free Sarcoplasmic Reticulum
6. **HERG** Human EAG-Related Gene
7. **JLN** Jervell and Lang-Nielsen Syndrome
8. **jSR** Junctional Sarcoplasmic Reticulum
9. **LQTS** Long QT Syndrome
10. **LQT2** Long QT Syndrome Type 2
11. **QTc** Rate Corrected QT Interval
12. **RyR2** Cardiac Ryanodine Receptor
13. **SR** Sarcoplasmic Reticulum
14. **CL** Cycle Length

ACKNOWLEDGEMENTS

My past two years at Youngstown State University have been both challenging and rewarding. I know I would not have been able to accomplish all that I have without the special people in my life that keep me inspired and motivated.

I would like to dedicate my thesis to Dr. Carl Sims. He was not only my advisor but grew to become my friend. He will certainly be missed. Dr. Sims was one of the most patient and understanding people I encountered since my time at YSU and for that I will always be appreciative. Thank you for always taking the time to explain everything to me and being there to answer all of my questions. He not only taught me much about his field of study but also taught me how to work well with others. I will never forget all of the funny conversations we had while driving back and forth to NEOUCOM, he definitely made research fun for me! I will never forget the impact he had on my life.

I would also like to thank my committee members, Dr. Jill Tall, Dr. Mark Womble, and Dr. Jozsi Jalics. Dr. Tall, thank you for being not only someone I can look up to as a role model but also someone I knew I could talk to if I needed anything. Dr. Womble, thank you for being there when I had any questions and taking the time to revise my thesis over and over and over. I will never look at a red pen the same way again! Dr. Jalics thank you for stepping in when I needed you, it will never be forgotten. I would like to thank all of the undergraduates who helped me with this project, especially Zane Kalik. Thank you for keeping me sane during those long hours of patch clamping. My friends and fellow graduate students helped me through everything, without them I surely would not have been able to complete this degree.

Last, but certainly not least, I would like to thank my family for always supporting me in everything that I do. I know that without them I would not be where I am today and for that I will always be thankful.

CHAPTER 1

I. Introduction

A. Cardiac Action Potential

The classic model of the cardiac action potential consists of five phases (0-4) and is generated by the ion currents I_{Na}, $I_{Ca\text{-}L}$, I_{NCX}, I_{K1}, I_{to}, I_{Kr}, and I_{Ks} (Figure 1). Phase 4 is referred to as the resting membrane potential, which in cardiac cells is around -80 mV to -90 mV (Camm et al. 2004). During the resting membrane phase, the membrane potential is dependent on the actions of Na/K ATPase and the inward rectifier potassium current (I_{K1}). Phase 0 of the action potential is characterized by the rapid depolarization of the cell. Depolarization of a cardiac myocyte is usually initiated by a current spread from nearby active regions (Bers 2001b). The rapid opening of the large inward sodium current (I_{Na}) and then the L-type calcium current ($I_{Ca\text{-}L}$) depolarizes the membrane potential from its resting level of near -80 mV to a peak value of approximately +30 mV (Camm et al. 2004). At the peak of the cardiac action potential (phase 1), the sodium channels rapidly close and there is an opening of a transient outward potassium channel (I_{to}), causing a slight repolarization. Phase 2 consists of a plateau, which prolongs the duration of the action potential. Depolarization during the plateau phase is maintained by the inward L-type calcium current (Camm et al. 2004). The prolonged plateau is the feature that distinguishes the cardiac action potential from action potentials in neurons or skeletal muscle cells. Phase 3 of the cardiac action potential occurs when the L-type calcium channels inactivate and the slow and rapid delayed rectifier potassium currents are activated, causing an increase in potassium conductance. The slow delayed rectifier potassium current (I_{Ks}) activates more slowly while the rapid delayed rectifier potassium

current (I_{Kr}) increases as the process of repolarization progresses (Bers 2001a). The increase in potassium conductance causes the membrane to repolarize (Moss et al. 2005), restoring the cell to resting potential state (phase 4) of -80 to -90 mV.

B. Early After-Depolarization

An afterdepolarization is a form of transient depolarization that can occur during two distinct phases of a cardiac action potential. An early afterdepolarization (EAD) occurs during the plateau phase of the cardiac action potential and a delayed afterdepolarization (DAD) occurs during phase 4 of the cardiac action potential (Gyorke et al. 2008). EADs are more commonly seen at slow heart rates and DADs are more commonly seen at fast heart rates.

Two major cellular mechanisms have been suggested in the generation of EADs. The first mechanism involves reactivation of the L-type calcium current under conditions of extended action potential duration due to reductions in K^+ conductance. However, the exact mechanism underlying EAD genesis is unknown (January et al. 1989). When repolarization is delayed, the plateau phase (phase 2) of the cardiac action potential is prolonged. The delay in repolarization can be caused by reductions in the potassium currents. I_{Kr} and I_{Ks}, which are responsible for restoring the membrane back to the resting membrane potential value of ~ -80 mV. Prolongation of the plateau phase of the action potential allows the L-type calcium channel to recover from inactivation. Because the membrane potential of the cell is still at a depolarized level, the L-type calcium current ($I_{Ca\text{-}L)}$ can reactivate, resulting in a second depolarization, which is seen as an EAD (Patterson et al. 2006).

The second mechanism that may be responsible for EAD production involves intracellular calcium homeostasis. The sarcoplasmic reticulum (SR) of cardiac myocytes is a highly specialized form of endoplasmic reticulum, which serves as an intracellular calcium storage site. Calcium release must be highly regulated in order to insure proper cardiac health. Alterations in the amount of calcium released or the time at which the calcium is released from the SR can lead to arrhythmias and heart failure (Gyorke et al. 2008). The release of calcium from the SR is controlled by a cardiac ryanodine receptor (RyR2) and other accessory proteins.

The SR consists of two regions, the junctional SR (jSR) and the free SR (fSR). Calcium release from the jSR is initiated by calcium binding to the RyRs. Once the calcium enters the cell, via the L-type calcium channel, calcium release channels located in the jSR will be activated by the Ca^{2+} binding to RyRs. That activation will in turn amplify the initial calcium signal and will produce an elevation of intracellular Ca^{2+} concentration throughout the cell, also known as the Ca^{2+} transient. The increase in Ca^{2+} concentration will lead to the generation of a cardiac muscle contraction via Ca^{2+} binding to troponin and initiating the sliding filament mechanism.

An abnormal release of Ca^{2+} from the SR has been thought to cause a wide range of heart diseases under conditions of prolonged action potential duration (APD). An abnormal increase of Ca^{2+} in the SR will lead to Ca^{2+} overload and the spontaneous release of Ca^{2+} from the SR. This Ca^{2+} release can result in the stimulation of the Ca^{2+}-activated inward current (I_{NCX}) that is generated by the forward mode of the sodium-calcium exchange (NCX). I_{NCX} can help prolong APD and generate a depolarizing current sufficient to cause an EAD (Patterson et al. 2006).

C. L Type Calcium Channel

Voltage gated calcium channels are present in cardiac, smooth, and skeletal muscle (Catterall 2000). Different types of calcium currents have been identified by physiological, pharmacological, and biophysical properties and include the L-type, N-type, P-type, Q-type, R-type, and T-type calcium currents. The two types of calcium currents found in cardiac tissue are the L-type and T-type calcium currents. T-type calcium channels are low voltage activated and transient (Perez-Reyes et al. 1998). This discussion will focus on the high voltage activated L-type calcium channel, which is the most prominent calcium channel found in the heart (Bers 2001b).

The L-type calcium channel is activated during the cardiac action potential when the membrane is depolarized to around -40 mV (Catterall 2000; Sims et al. 2004). Once the channel is activated, calcium moves down its concentration gradient and into the myoplasm. As calcium enters the cardiac myocyte via the L-type calcium channel, this induces the release of more calcium from the sarcoplasmic reticulum and the contraction process begins (Mukherjee et al. 1998). Inactivation of the calcium current is slow and dependent on voltage and intracellular calcium concentration. When intracellular calcium concentration is increased it causes inactivation of the calcium current. If the voltage of the cell is more negative than -40 mV, the channel begins to close.

The voltage gated L-type calcium channel of the heart is comprised of four subunits (Figure 2). The subunits are α_{1c}, α_2/δ, and β (Bodi et al. 2005). The α_1 subunit (170-240 kDa) is the primary subunit of the calcium channel and the α_2/δ and β are accessory subunits which are tightly bound to the α_1 subunit (Bodi et al. 2005). The pore forming subunit, $\alpha_{1,}$ is composed of four homologous regions (I, II, III, IV), with each

consisting of six transmembrane sequences (Ding et al. 1999; Keef et al. 2001; Bodi et al. 2005). The α_1 subunit has been characterized into four separate classes located in distinct tissues, $Ca_v1.1$ (α_{1S}) is located in skeletal muscle, $Ca_v1.2$ (α_{1C}) is located in cardiac muscle, endocrine cells, and neurons, $Ca_v1.3$ (α_{1D}) is located in endocrine cells and neurons, and Ca_v 1.4 (α_{1F}) is located in the retina. The $Ca_v1.2a$ (α_{1C}) subunit is the only one highly expressed in cardiac tissue. The α_{1c} amino acid sequence in the rabbit was found to be 2,171 amino acids long (Ding et al. 1999). Cysteine residues are found throughout the entire length of the subunit and may provide sites for redox regulation (Sims et al. 2004).

The α_2/δ is an accessory subunit to the α_1 subunit. The δ subunit spans the myocyte cell membrane and anchors the α_2 subunit to it by a disulfide bond (Jay et al. 1991). The α_2 subunit is thought to be important for regulating the level of expression of functional channels. The δ subunit may be responsible for regulating channel gating properties (Gurnett et al. 1996). The β subunit (β_2 subunit in cardiac tissue) is located between the I and II homologous region of the α_1 subunit. The molecular mechanism of the binding of the β subunit to the α_1 subunit is still in question. It is known that the β subunit directs the α_1 subunit to the membrane and regulates channel activation and inactivation kinetics. The β subunit is also believed to enhance the L-type calcium current ($I_{Ca\text{-}L}$) during β–adrenergic regulation of α_{1C}.

D. Electrocardiogram (ECG)

The electrocardiogram is a graphical way to represent what is occurring in the cardiac cells. The electrical currents generated by action potentials moving across the myocardium can be recorded by surface electrodes to produce an ECG. The ECG is

composed of a series of waves, with each wave representing a different event that occurs during the cardiac cycle. The waves that compose the normal ECG are the P wave, QRS complex, and T wave (Figure 3A). The ECG can be further defined in intervals, PR interval, QRS interval, ST interval, TR interval, QT interval, and RR interval.

The P wave is the first deflection in the normal ECG and represents atrial depolarization, which results in the contraction of the atria (Merri et al. 1989). The QRS complex consists of the Q wave, R wave, and S wave and represents ventricular depolarization. The ventricular depolarization will result in the contraction of both ventricles. The T wave is the last deflection of the normal ECG and represents ventricular repolarization. This wave is associated with the relaxation of the ventricles.

The QT interval is the interval of interest in this study. A normal QT interval is depicted in Figure 3A. The QT interval is defined as the time from the start of the Q wave to the end of the T wave. This interval represents the time it takes for the ventricular depolarization and repolarization to occur and thus represents the duration of the ventricular action potential. Therefore, if repolarization is delayed there will be an extended QT interval, as shown in figure 3B, and the ventricular action potential will be prolonged.

E. Long QT Syndrome

The leading cause of death in the United States for both men and women is heart disease. Long QT Syndrome (LQTS) is a unique type of heart defect that may be congenital or acquired and can result in sudden death. Patients with LQTS are at a much higher risk of experiencing ventricular arrhythmias. LQTS may be congenital due to a specific genetic mutation, or acquired, resulting from drug interactions with cardiac ion

channels. However both forms of LQTS result in an extended QT interval. Commonly, the QT interval is spoken of in terms of the rate corrected QT interval or QTc. This simply takes into account the heart rate of the individual when measuring the QT interval and is calculated by take the QT interval and dividing it by the square root of the RR interval. The RR interval is the time between ventricular depolarizations and thus represents one heart beat. Heart rate must be taken into account because it is known that women experience faster resting heart rates than men. The average resting heart rate of females is 69 ± 0.126, while the average heart rate of males is 63 ± 0.146 (Merri et al. 1989). While the normal QTc interval is between 350 and 460 msec, the mean QTc interval for those who suffer from LQTS, in both men and women, is 480 msec, (Vincent et al. 2002). To allow for the diagnosis of LQTS, men must have a QTc ≥ 470 msec and women must have QTc ≥ 480 msec (Vincent et al. 2002).

F. Congenital Long QT Syndrome

Congenital LQTS is now recognized as consisting of four different syndromes: Romano-Ward, Jervell and Lang-Nielsen (JLN), Anderson, and Timothy syndromes. Romano-Ward syndrome is characterized by a family occurrence with autosomal dominant inheritance, QT prolongation, and ventricular arrhythmias (Vincent et al. 2002). JLN syndrome is characterized by a family occurrence with autosomal recessive inheritance, congenital deafness, QT prolongation, and arrhythmias (Vincent et al. 2002). All four types of these syndromes are caused by a genetic mutation in a cardiac potassium, sodium, or calcium channel, or a channel associated protein. However about 95% of cases involve mutation of a potassium channel (Vincent et al. 2002). Thus far twelve different susceptible genes have been identified, including 10 types of Romano-

Ward syndrome (LQT1-6), 2 types of JLN syndrome (JLN1-2), 1 type of Anderson syndrome, and 1 type of Timothy syndrome (Table 1) (Hedley et al. 2009).

The congenital forms of LQTS cause 2000-3000 sudden deaths in children and young adults each year in the United States (Vincent et al. 2002). Long QT Syndrome Type 2 (LQT2) is the second most common form of LQTS. The gene associated with LQT2 is the human eag-related gene (HERG) which encodes the I_{Kr} channel that carries the rapid component of the delayed rectifier potassium current in cardiac myocytes (Vincent et al. 2002). A study conducted by Curran et al. in 1995 confirmed that LQT2 was linked to markers on the chromosome 7q35-36. They were also able to conclude that HERG also mapped to chromosome 7q35-36. This suggests that HERG is linked to LQT2. The I_{Kr} current is responsible for repolarizing the membrane during an action potential (Moss et al. 2005). If this channel is mutated, the cell will not repolarize correctly, resulting in the prolongation of the ventricular action potential and a prolonged QT interval.

G. Acquired Long QT Syndrome

Similarly, the acquired form of LQTS also results in a longer QT interval through the blockage of the normal outward rapid component of the delayed rectifier potassium current (I_{Kr}) by different types of drugs (Vincent et al. 2002). Antiarrhythmic medications are the most commonly known drugs that cause this type of disorder. However, many types of noncardiac drugs are also known to cause QT prolongation and arrhythmias. Examples of noncardiac drugs include antihistamines, antipsychotics, and antibiotics (Camm et al. 2004). There were many suggestions as to the mechanism of prolonging the QT interval, however, it has been recognized that the blockage of I_{Kr} results in the

slowing of repolarization and the prolongation of the ventricular action potential and thus a lengthening of the QT interval (Camm et al. 2004).

Acquired LQTS can also be associated with other conditions and may not necessarily be drug-induced. Certain cardiac conditions are known to cause a prolonged QT interval. In 1978, Schwartz and Wolf demonstrated that the QT interval is significantly prolonged after a subject experiences a myocardial infarction when compared to control subjects. Other studies have also shown that dilated cardiomyopathy, congestive heart failure, hypertrophic cardiomyopathy, hypertension, bradycardia, myocarditis, and Kawasaki syndrome can all cause acquired LQTS (Camm et al. 2004). Noncardiac conditions, such a diabetes mellitus, are also known to cause acquired LQTS (Camm et al. 2004). Other conditions linked to a longer QT interval include obesity, anorexia nervosa, hypokalaemia, hepatic failure, intracranial hemorrhage, and hypothyroidism.

Female sex is also a risk factor for acquired LQTS (Camm et al. 2004). Several studies examined patients who were treated with antiarrhythmic drugs to determine if an arrhythmia arose. A study conducted by Lehmann et al. (1996) surveyed 3135 patients that were treated with d,1-sotalol, an beta-adrenergic antagonist drug that prolongs the duration of the action potential. They concluded that 4% (33/799) of women but only 1.8% (44/2336) of men experienced an arrhythmia, a significant difference. Another study by Ebert et al. (1998) used adult male and female rabbit hearts to determine whether gender differences exist between changes in QT duration in response to two different drugs, quinidine and d,1-sotalol. They concluded that females displayed greater drug-induced QT interval increases and had a significantly lower I_{Kr} current density.

However, there is still much to be determined about the effects of gender differences in acquired LQTS.

H. Sex, Age, Hormonal Regulation, and Long QT Syndrome

Sex is an important factor when discussing the QT interval and more specifically the QTc. It is known that women have a longer QTc than men and are more vulnerable to the life threatening arrhythmias associated with LQTS. Studies have shown that women have smaller I_{K1}, I_{Ks} and I_{Kr} current densities in ventricular myocytes when compared to men (Cheng et al. 1999). Those currents are responsible for returning the cardiac cell to the resting membrane potential. Thus, this data suggests that women have longer QTc intervals due to lower levels of these potassium currents. A study conducted by Bazett (1920) reported that women have a 6% longer QTc interval than men. It is known that androgen, specifically testosterone, is responsible for the shortening of the QT interval in males following puberty (Pham et al. 2002). However, as men age and circulating testosterone levels decrease, their QTc interval increases (Pham et al. 2002). It has been concluded that men and women have relatively the same QTc interval around age 50 (Pham et al. 2002). Thus, potassium current density has proven to be one factor when considering sex differences in QTc interval and the lethal arrhythmias associated with interval prolongation.

In 2005, Liu et al. reported that pre-pubertal male rabbits with drug-induced LQT2 are more susceptible to deadly arrhythmias when compared to age-matched females. However, pre-pubertal females still showed longer action potential durations. Therefore, factors other than action potential duration, hormonal regulation, and potassium current density must also regulate arrhythmia vulnerability. One such factor

may be L-type calcium current ($I_{Ca\text{-}L}$). Sims et al. (2008) reported that myocytes taken from the base region of the pre-pubertal rabbit left ventricle exhibited higher $I_{Ca\text{-}L}$ levels when compared to male apex cells or myocytes from either the base or apex of pre-pubertal females. This suggests that the arrhythmias observed by Liu et al. (2005) may be associated with higher levels of $I_{Ca\text{-}L}$.

Additional evidence for this possibility comes from studies of adult rabbit apex and base myocytes. In adult rabbits, the sex difference in $I_{Ca\text{-}L}$ levels is reversed, so that adult female left ventricle base myocytes exhibit the highest current levels when compared to female apex or male apex and base myocytes (Sims et al. 2008). This suggests that the difference in calcium current density levels may be a contributing factor to a women's heightened EAD genesis propensity.

Gender related differences in transmural dispersion of the L-type calcium current have also been examined. Pham et al. (2002) studied control male and female adult rabbits and hormonally-treated castrated male and female adult rabbits. The two hormones used were 5α-dihydroxytestosterone (DHT) and 17β-estradiol (EST), given to both sexes. The researchers concluded that female rabbits showed a greater density of $I_{Ca\text{-}L}$ in the epicardial region of the myocardium versus the deeper myocardium region, when DHT and EST were administered. Age-matched males did not show any significant differences in $I_{Ca\text{-}L}$ (Pham et al. 2002). These findings suggest that there are gender differences in the mechanism of action of both hormones and the greater $I_{Ca\text{-}L}$ dispersion in the myocardium of females may contribute to gender differences in repolarization.

Sex differences in the expression of the L-type calcium channel have also been demonstrated. In rats, the ventricular tissue of females exhibits a greater quantity of

L-type calcium channel expression than age-matched males and this correlates with sex differences in force generation (Chu et al. 2005). The L-type calcium current density in the right ventricle of rabbits will be examined in this study as a potential factor in contributing to the sex differences in deadly arrhythmia generation.

The three major gonadal steroid hormones thought to play an important role in regulating cardiac ion channels are estrogen, progesterone, and testosterone. All three are produced through similar biosynthetic pathways from the common precursor pregenolone. The mechanism responsible for sex differences in arrhythmia vulnerability is still not known. The majority of the studies conducted have focused on the hormonal regulation of K^+ channel changes and their involvement in phase 3 of the cardiac action potential.

A study by Cheng et al. (1999) reported a higher distribution of I_{Kr} in adult male compared to adult female ventricular myocytes. The authors suggest that the sex differences seen in QTc were due to ion channel distribution and not to hormonal regulation. A study contradicting these results reported that testosterone in males stimulates the expression of I_{Kr}, which would therefore enhance the repolarization reserve and decreases the QTc. This study also concluded that estrogen in females blocked potassium channels, causing the repolarization reserve to lessen and therefore increase the QTc (Pham et al. 2001).

Studies investigating sex hormone modulation of $I_{Ca\text{-}L}$ have produced no consistent theme. Bai et al. (2005) reported that testosterone induces the production of nitric oxide which suppressed the L-type calcium current via a cGMP activation of a cAMP sensitive phosphodiesterase. Progesterone prevents the enhancement of $I_{Ca\text{-}L}$ and

estrogen inhibits the cardiac ion current $I_{Ca\text{-}L}$ (Nakamura et al. 2007; Berger et al. 1997; Gupte et al. 2002; Nakajima et al. 1999).

I. Goals of this Study

Results from previous studies suggest that factors other than hormonal regulation of ion currents and APD are responsible for sex differences in arrhythmia vulnerability in LQTS. In adult rabbit heart, differences in sex and apex-base $I_{Ca\text{-}L}$ levels in left ventricle myocytes were correlated with gender differences in EAD vulnerability. Sex and regional differences in $I_{Ca\text{-}L}$ levels in the right ventricle of adult rabbit hearts have not been studied. Therefore, the goal of this study is to use the whole cell patch clamp technique to examine whether sex and apex-base differences in $I_{Ca\text{-}L}$ levels exist in right ventricle myocytes of adult rabbits. Experimental findings will be incorporated into cardiac AP simulations to determine the role of the L-type calcium current in regulating APD and membrane potential in healthy and diseased hearts. These studies will assist in expanding our understanding of the distribution of ion current levels in the heart and help to characterize their role in repolarization associated heart diseases such as LQTS.

Specific Aim 1:

To determine if sex and apex-base differences in $I_{Ca\text{-}L}$ levels exist in the myocytes of the adult rabbit right ventricle. Currents from apex and base myocytes will be measured by the whole cell patch clamp technique. Experimentally determined gender and regional differences in current densities and voltage-dependent parameters for $I_{Ca\text{-}L}$ will be incorporated into the Luo-Rudy action potential model and simulations will be performed under conditions that mimic LQT2 to predict EAD sensitivity.

Table 1: Different Types of Long QT Syndrome, Mutated Gene Associated, and Ion Current Affected

Type of LQTS	**Chromosomal Locus**	**Mutated Gene**	**Ion Current Affected**
LQT1	11p15.5	*KVLQT1, or KCNQ1*	Potassium (I_{Ks})
LQT2	7q35-36	*HERG, KCNH2*	Potassium (I_{Kr})
LQT3	3p21-24	*SCN5A*	Sodium (I_{Na})
LQT4	4q25-27	*ANK2, ANKB*	Sodium, Potassium and Calcium
LQT5	21q22.1-22.2	*KCNE1*	Potassium (I_{Ks})
LQT6	21q22.1-22.2	*MiRP1, KNCE2*	Potassium (I_{Kr})
LQT7	17q23.1-q24.2	*KCNJ2*	Potassium (I_{K1})
LQT8	12q13.3	*CACNA1C*	Calcium ($I_{Ca\text{-}Lalpha}$)
LQT9	3p25.3	*CAV3*	Sodium (I_{Na})
LQT10	11q23.3	*SCN4B*	Sodium (I_{Na})
LQT11	7q21-q22	*AKAP9*	Potassium (I_{Ks})
LQT12		*SNTAI*	Sodium (I_{Na})
JLN1	11p15.5	*KVLQT1, KCNQ1*	Potassium (I_{Ks})
JLN2	21q22.1-22.2	*KCNE1*	Potassium (I_{Ks})

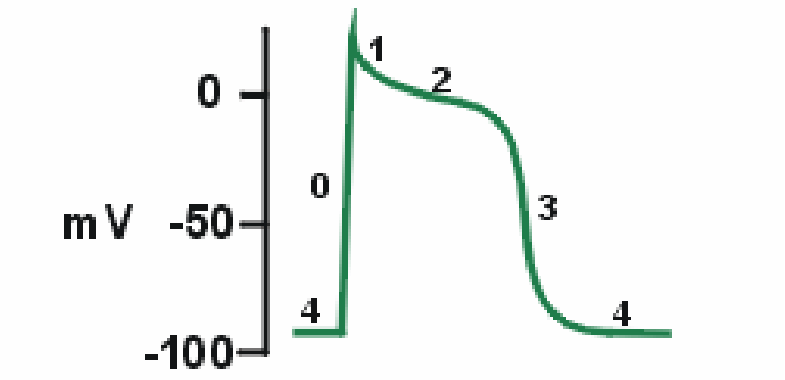
0
mV
-50
-100
0
1
2
3
4
4

Figure 1: Cardiac Action Potential – This figure represents a normal ventricular cardiac action potential. The classic model of the cardiac action potential consists of five phases (0-4) and is generated by the ion currents I_{Na}, $I_{Ca\text{-}L}$, I_{NCX}, I_{K1}, I_{to}, I_{Kr}, and $I_{Ks.}$ Phase 4 is referred to as the resting membrane potential, which in cardiac cells is around -80 mV to -90 mV. Phase 0 of the action potential is characterized by the rapid depolarization of the cell. The large and rapid opening of the inward sodium current (I_{Na}) and then the L-type calcium current ($I_{Ca\text{-}L}$) changes the membrane potential from -90 mV to approximately +30 mV. Phase 2 consists of a plateau, which prolongs the duration of the action potential. This phase is produced by continued activation of $I_{Ca\text{-}L}$. Phase 3 of the cardiac action potential occurs when the L-type calcium channels inactivate and there is an increase in potassium conductance of the cell with activation of I_{Kr} and I_{Ks}. After the cell repolarizes, it is restored to it resting potential state (phase 4). This figure was taken from the website http://www.cvpharmacology.com/antiarrhy/cardia1.gif.

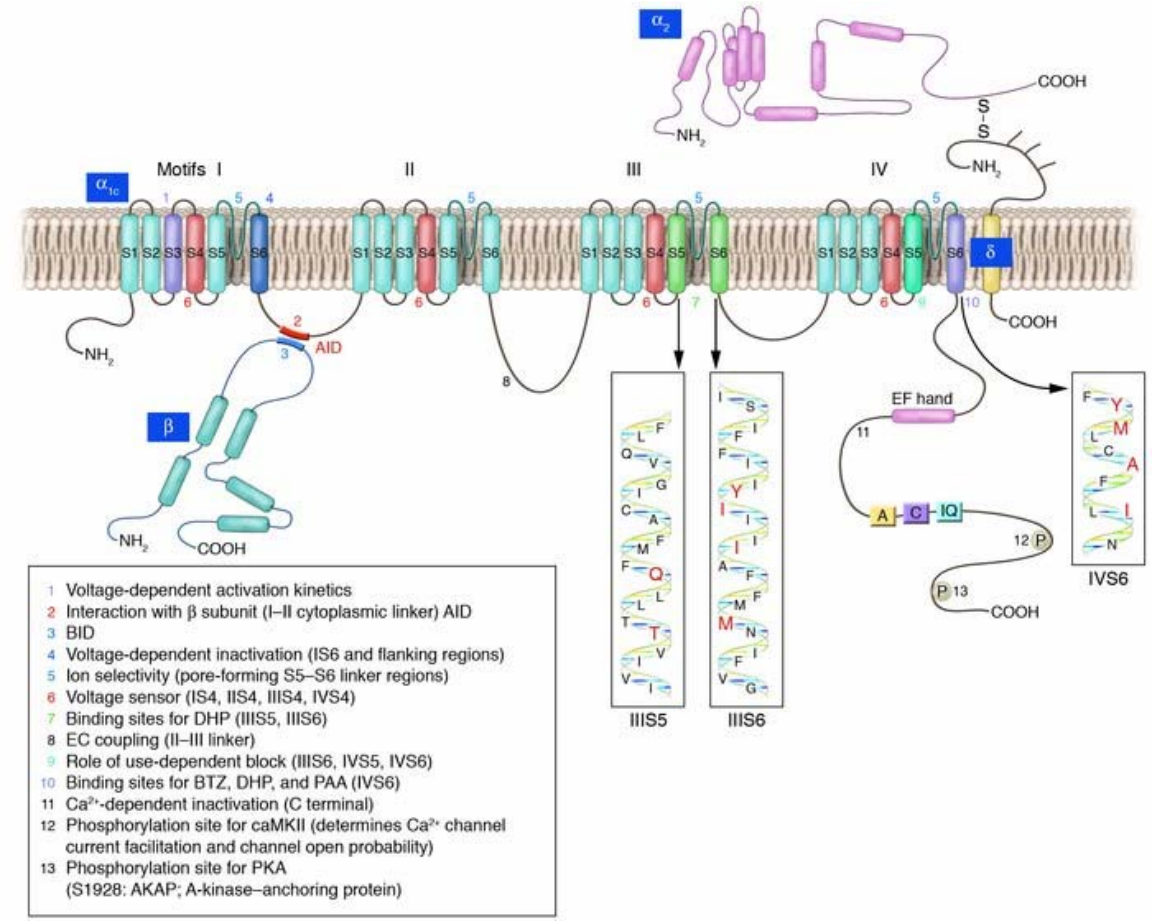
α2
COOH
S
S
NH2
Motifs I
II
III
IV
α1c
S1 S2 S3 S4 S5 S6
δ
NH2
COOH
AID
β
NH2
COOH
EF hand
A C IQ
12 P
P 13
COOH
IVS6
IIIS5
IIIS6
1 Voltage-dependent activation kinetics
2 Interaction with β subunit (I–II cytoplasmic linker) AID
3 BID
4 Voltage-dependent inactivation (IS6 and flanking regions)
5 Ion selectivity (pore-forming S5–S6 linker regions)
6 Voltage sensor (IS4, IIS4, IIIS4, IVS4)
7 Binding sites for DHP (IIIS5, IIIS6)
8 EC coupling (II–III linker)
9 Role of use-dependent block (IIIS6, IVS5, IVS6)
10 Binding sites for BTZ, DHP, and PAA (IVS6)
11 Ca2+-dependent inactivation (C terminal)
12 Phosphorylation site for caMKII (determines Ca2+ channel current facilitation and channel open probability)
13 Phosphorylation site for PKA (S1928: AKAP; A-kinase–anchoring protein)

Figure 2: Depiction of the L-type Calcium Channel - The voltage gated L-type calcium channel of the heart is comprised of four subunits, α_{1c}, α_2/δ, and β. The α_1 subunit (170-240 kDa) is the primary subunit of the calcium channel and the α_2/δ and β are the accessory subunits which are tightly bound to the α_1 subunit. The pore forming subunit, $\alpha_{1,}$ is composed of four homologous regions (I, II, III, IV), with each consisting of six transmembrane sequences. The α_{1c} amino acid sequence in the rabbit was found to be 2,171 amino acids long. The α_2/δ is an accessory subunit to the α_1 subunit. It is known that the β subunit directs the α_1 subunit to the membrane and regulates channel activation and inactivation kinetics. The β subunit is also believed to enhance the L-type calcium current ($I_{Ca\text{-}L}$) during β–adrenergic regulation of α_{1C}. This figure was taken from the reference Bodi et al. 2005.

A)

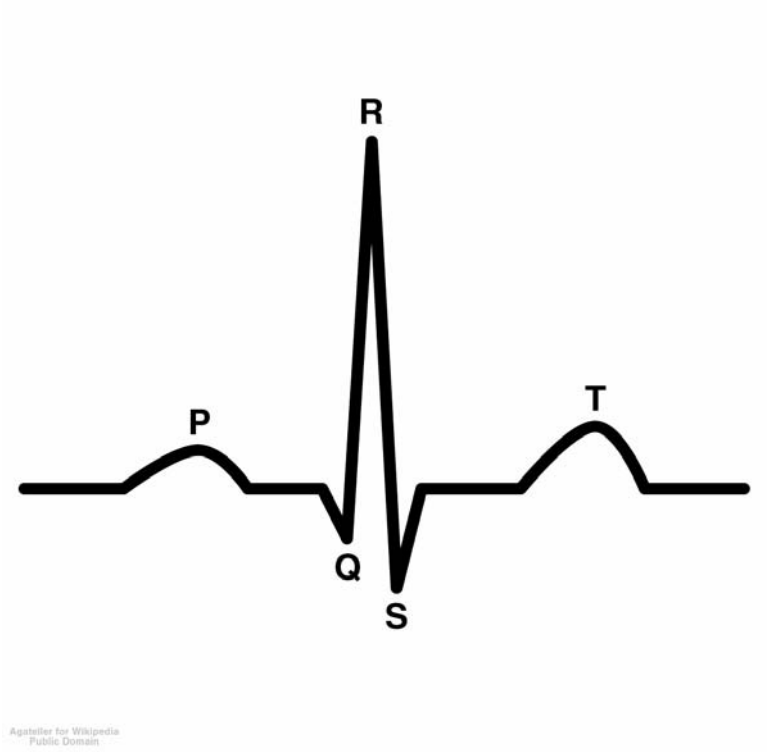
R
P
T
Q
S
Agateller for Wikipedia
Public Domain

B)

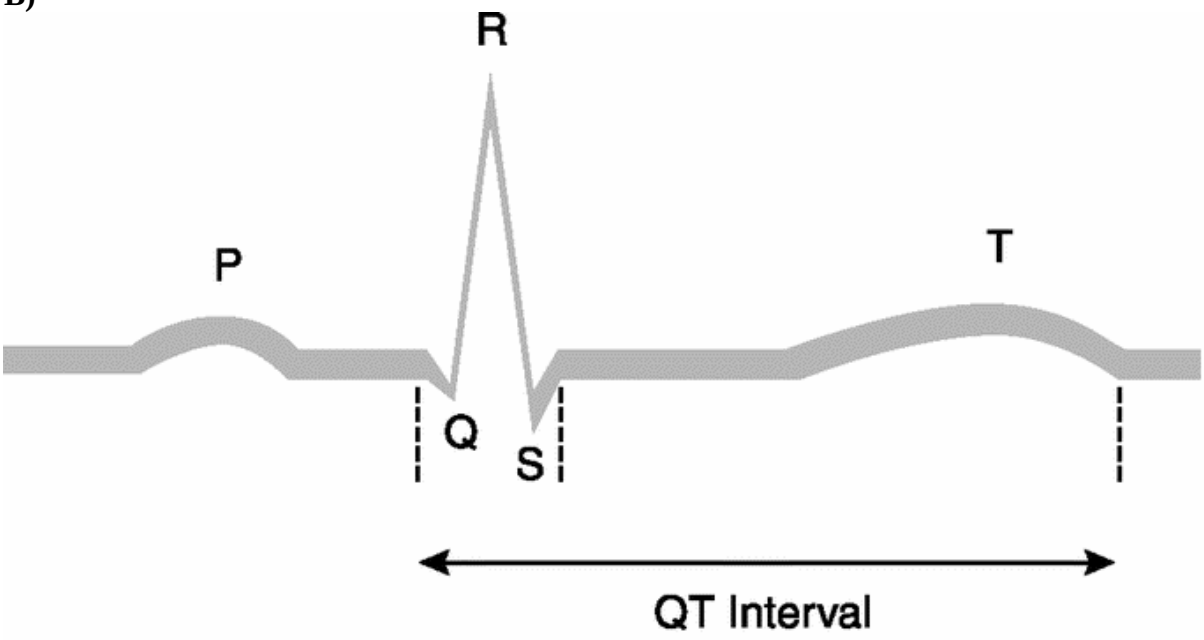
R
P
T
Q
S
QT Interval

Figure 3: Electrocardiograms (ECGs) – A) Normal Electrocardiogram - The electrical currents generated by action potentials moving across the myocardium are recorded by surface electrodes as an electrocardiograph. The ECG is composed of a series of waves with each wave representing a different event that occurs during the cardiac cycle. These waves are the P wave, QRS complex, and T wave. This figure was taken from the website http://www.vanth.org/vibes/electro.html. **B)** Electrocardiogram Showing Prolonged QT Interval - The QT interval is defined as the time from the start of the Q wave to the end of the T wave. This interval represents the time it takes for the ventricular depolarization and repolarization to occur. Therefore, if ventricular repolarization is delayed due to a prolonged action potential there will be an extended QT interval. This figure was taken from the website http://wiki.medpedia.com/Image:LongQT_f1.gif?filetimestamp=20081214040514.

CHAPTER 2

II. Materials and Methods

A. Cell Isolation

Cardiac myocytes were isolated from adult New Zealand White Rabbits of either sex. The animals were anesthetized through an intravenous injection in the ear vein with pentobarbital (50mg/kg), followed by heparin (1,000 U/kg). Once confirming the animals were properly anesthetized, the heart was surgically removed and placed on a Langendorf perfusion apparatus. An oxygenated Ca^{2+} -containing physiological salt solution (PSS) containing (in mM): 140 NaCl, 5.4 KCl, 1.5 $CaCl_2$, 2.5 $MgCl_2$, 11 glucose, and 5.5 HEPES (pH 7.6) was perfused through the heart via the aorta for five minutes at 39ºC at a rate of 16 ml/min. The solution was then switched to Ca^{2+} -free PSS for ten minutes. The next solution perfused through the heart was Ca^{2+} free PSS containing collagenase (0.01 g/ml) for fifteen minutes. After digestion of the heart was completed, the solution was switched back to Ca^{2+} free PSS solution to wash out the collagenase. The heart was then removed from the apparatus and placed in potassium buffer (KB) solution containing (in mM): 110 potassium glutamate, 10 KH_2PO_4, 25 KCl, 2 $MgSO_4$, 20 taurine, 5 creatine, 0.5 EGTA, 20 glucose, and 5 HEPES (pH 7.4). The heart was dissected into separate right ventricle apex and right ventricle base regions. To acquire single cardiac myocytes, the digested tissue was minced and filtered through a 210 micron nylon mesh. Adequate time was given for the cells to settle before the supernatant was removed and the cells were then resuspended in KB solution. The cells were left in KB solution at room temperature until needed. The methods used in this procedure were approved by the Institutional Animal Care and Use Committee at Youngstown State University.

B. Data Acquisition and Analysis

The conventional whole cell configuration of the patch clamp technique (Hamill et al. 1981) was used to study the L-type Ca^{2+} current. Microelectrodes were pulled from 100 µL micropipettes (VWR Scientific, Westchester, PA) and had a resistance between 0.7 and 2.5 MΩ when filled with an intracellular solution containing (in mM): 130 CsCl, 20 tetraethylammonium chloride (TEA-Cl), 5 MgATP, 5 EGTA, 0.1 TRIS-GTP, and 5 HEPES (pH 7.2). Cells were bathed in a K^+-free control extracellular solution containing (in mM): 140 NaCl, 5.4 CsCl, 2.5 $CaCl_2$, 0.5 $MgCl_2$, 11 glucose, and 5.5 HEPES (pH 7.4). Macroscopic currents were recorded using an Axopatch 200B voltage-clamp amplifier (Molecular Devices, Sunnyvale, CA) and a Dell computer with a Digidata 1440A interface and pCLAMP software (Molecular Devices, Sunnyvale, CA).

Isolated cardiac myocytes were placed in a 1 mL chamber on the stage of an inverted microscope where they were superfused with the extra-cellular potassium free solution at a rate of 1 to 2 ml/min. All experiments were performed at room temperature. The L-type Ca^{2+} current was isolated by inactivating the Na^+ current with a voltage clamp prepulse to -30 mV, blocking K^+ currents with Cs^+ and TEA, and measuring the Ca^{2+} current near the adjusted equilibrium potential for Cl^- (0 mV), thereby eradicating the driving force of Cl^-.

A voltage protocol was used to measure the calcium current conductance in male and female apex and base cells. Myocytes were voltage-clamped at a holding potential of -80 mV. A 40 ms prepulse to -30 mV was applied to activate and deactivate the voltage-gated Na^+ current. This was followed by a 100 ms step to 0 mV to activate the Ca^{2+} current, during which the peak Ca^{2+} current and time course of changes in current

amplitude were recorded. This voltage step protocol was repeated every 5 seconds. Once the data was collected, statistical analysis was conducted. The student t-test was used to determine significance, $p<0.05$. All data given as mean ± S.E.M.

Activation and inactivation properties of $I_{Ca\text{-}L}$ were also determined. Parameters for the voltage dependence of activation were obtained from the least squares fit of data points to the equation: $g/g_{max} = 1/(1 + \exp -((V_T – V_{0.5})/b))$, where g/g_{max} represents the normalized Ca^{2+} conductance, V_T represents test potentials from -30 to 30 mV, $V_{0.5}$ is the potential at which activation was half maximal, and b is the slope. The conductance at each test potential was calculated using the reversal potential (V_r) obtained from the current voltage relationship measured under each voltage step of the activation protocol. Conductance = ((Current density)/(V_T-V_r)).

Parameters for the voltage dependence of inactivation were obtained from the equation: $I = I_{ir} + (1 - I_{ir})/(1 + \exp -((V_c - V_{0.5})/b))$, where I is the normalized magnitude of the peak inward current measured during a test pulse to 0 mV following a 5 sec conditioning pulse (V_c) to membrane potentials between -50 and 20 mV, I_{ir} is the inactivation resistant current, $V_{0.5}$ is the potential at which inactivation was half maximal, and b is the slope. The current elicited during the test pulse was normalized to the magnitude of the current recorded during a pretest pulse to 0 mV, which preceded each conditioning pulse.

C. Mathematical Modeling

Right ventricular action potentials were simulated using a modified version of the Luo-Rudy cardiac AP (Faber et al. 2000). In this model, which incorporates the transient outward potassium current (I_{to}), membrane ion currents are mathematically represented

by the Hodgkin-Huxley formulation (Dumaine et al. 1999). The model also accounts for dynamic changes in intracellular calcium handling, which include Ca^{2+} release and uptake from the SR (including translocation of Ca^{2+} from network to junctional SR), Na^{+}/Ca^{2+} exchange, and Ca^{2+} buffering by calmodulin, troponin (in the cytoplasm) and calsequestrin (in the SR). Experimentally determined sex and regional differences in Ca^{2+} current densities were incorporated into the AP model by modifying the equations representing $I_{Ca\text{-}L}$. With these modifications, simulations were performed to examine the development of arrhythmogenic EADs with 50% I_{Kr} suppression by modifying its maximal conductance.

CHAPTER 3

III. Results

Sex and regional differences of the whole cell calcium current in acutely isolated cardiac myocytes obtained from the right ventricle of adult rabbits were examined in this study. The whole cell patch clamp technique was used to voltage clamp myocytes. Pharmacological and voltage protocols were used to eliminate Na^+, K^+, and Cl^- currents and thereby isolate the calcium current. The peak calcium current was recorded over a voltage range of -30 to +60 mV. Current responses and IV relationship data were used to analyze the differences in peak $I_{Ca\text{-}L}$ density between myocytes obtained from apex or base regions of the right ventricle in both male and female animals.

Isolated Ca^{2+} current responses were obtained by inactivating the Na^+ channel with a voltage clamp prepulse to -30 mV, blocking K^+ channels with Cs^+ and TEA, and measuring the Ca^{2+} current near the adjusted equilibrium potential for Cl^- (0 mV), thereby eradicating the driving force of Cl^-. The time course of changes in Ca^{2+} current amplitude was recorded by measuring the absolute magnitude of the peak inward current recorded during 100 ms voltage-clamp steps to 0 mV applied following a 40 ms prepulse to -30 mV from a holding potential of -80 mV once every 5 sec. Figures 4 and 5 show representative current tracings. Stepping to 0 mV results in the activation of a large inward L-type Ca^{2+} current which rapidly reaches its peak amplitude. The current then gradually inactivates and declines in amplitude throughout the remainder of the voltage step. Peak $I_{Ca\text{-}L}$ amplitudes were determined by placing cursors before and after the peak current and averaging the 5 most stable peak current amplitudes. Current amplitude was converted to current density by dividing the peak current amplitude of each cell by the

capacitance. Dividing the peak current amplitude by the capacitance of the cell allowed us to take into account the size of the cell and thus normalize the data.

Sex differences in $I_{Ca\text{-}L}$ density were observed in female versus male base myocytes (Figure 4). Adult female base myocytes (7.2±0.83 pA/pF, n=8) exhibited a 84.6% larger peak $I_{Ca\text{-}L}$ density when compared to male base myocytes (3.9±0.38, n=12, $p<0.001$). In apex myocytes, no significant difference was found in peak $I_{Ca\text{-}L}$ density between female (-4.56±0.45 pA/pF, n=9) and male (-4.31±0.58, n=4, $p<0.8$) myocytes.

Regional differences in Ca^{2+} current density were also found in female but not male myocytes (Figure 5). Female base myocytes showed a 56.5% larger peak $I_{Ca\text{-}L}$ density (7.2±0.83 pA/pF, n=8) compared to the female apex myocytes (-4.56±0.45 pA/pF, n=9, $p<0.02$). In males, no significant difference was found in peak $I_{Ca\text{-}L}$ density between apex myocytes (-4.31±0.58, n=4) and base myocytes (-3.87±0.38, n=12, $p<0.6$). These differences in the sex and regional distribution of Ca^{2+} current density are summarized in Figure 6.

Current-voltage (IV) relationships for the peak $I_{Ca\text{-}L}$ density were obtained from myocytes by stepping from a holding potential of -80 mV to step potentials of -30 to +60 mV. As shown in Figures 7 and 8, $I_{Ca\text{-}L}$ activates beginning around -30 mV, with the peak $I_{Ca\text{-}L}$ density obtained at +10 mV. At more positive voltages, as the voltage begins to reach the equilibrium potential for calcium, the current begins to decline.

Maximum $I_{Ca\text{-}L}$ peak current densities were significantly larger at voltage values of 0 mV, +10 mV, and +20 mV in female base myocytes compared to male base myocytes (Figure 7A). Peak current densities for $I_{Ca\text{-}L}$ in male and female apex myocytes were similar over all voltages examined (Figure 7B). Maximum $I_{Ca\text{-}L}$ peak current

densities were similar in female base myocytes compared to female apex myocytes (Figure 8A) and male base myocytes when compared to male apex myocytes (Figure 8B) over all voltages examined. The maximum peak $I_{Ca\text{-}L}$ in female apex, male apex, and male myocytes were all similar, while the current density in female base myocytes was significantly larger.

One possible explanation for the large amplitude of $I_{Ca\text{-}L}$ observed in female base myocytes could be a difference in the voltage sensitivity of the current in these cells compared to male base or apex myocytes or female apex myocytes. However, this does not appear to be the case, since the IV plots shown in Figures 7 and 8 all show current activation at approximately -30 mV and peak current amplitudes at +10 mV for $I_{Ca\text{-}L}$ in all myocytes. To verify this conclusion, activation and inactivation properties of $I_{Ca\text{-}L}$ were directly measured. Parameters for the voltage dependence of activation were obtained from the least squares fit of data points to the equation: $g/g_{max} = 1/(1 + \exp -((V_T - V_{0.5})/b))$, where g/g_{max} represents the normalized Ca^{2+} conductance, V_T represents test potentials from -30 to 30 mV, $V_{0.5}$ is the potential at which activation was half maximal, and b is the slope. Parameters for the voltage dependence of inactivation were obtained from the equation: $I = I_{ir} + (1 - I_{ir})/(1 + \exp -((V_c - V_{0.5})/b))$, where I is the normalized magnitude of the peak inward current measured during a test pulse to 0 mV following a 5 sec conditioning pulse (V_c) to membrane potentials between -50 and 20 mV, I_{ir} is the inactivation resistant current, $V_{0.5}$ is the potential at which inactivation was half maximal, and b is the slope. The current elicited during the test pulse was normalized to the magnitude of the current recorded during a pretest pulse to 0 mV, which preceded each conditioning pulse.

Any differences in the activation and inactivation properties of $I_{Ca\text{-}L}$ observed in female base cells compared to other myocytes would suggest that other factors, such as an increase in the duration of channel opening, could be responsible for the increased magnitude in current density. However, no significant differences in $I_{Ca\text{-}L}$ activation and inactivation parameters were observed (Figure 9 and Table 2). Figure 9A shows the conductance-voltage relationship. As predicted from the IV curves shown in Figures 6 and 7, $I_{Ca\text{-}L}$ activated at approximately -30 mV and reached its peak conductance at +10 mV in all myocytes. Current inactivation in relation to membrane voltage is shown in Figure 9B. Prolonged (5 sec) conditioning voltage steps of -60 mV or more negative did not decrease the maximum amplitude of $I_{Ca\text{-}L}$ observed during the subsequent test voltage step. However, as the conditioning step was increased, current inactivation also increased and the observed maximum $I_{Ca\text{-}L}$ amplitude was reduced. Conditioning voltages above -30 mV completely inactivated $I_{Ca\text{-}L}$ prior to the test pulse, reducing the current amplitude to zero. No differences were found in inactivation among myocytes. These findings indicate that changes in the voltage dependency of $I_{Ca\text{-}L}$ activation or inactivation can not explain the large current density observed in female base myocytes.

Experimentally determined Ca^{2+} current densities of $I_{Ca\text{-}L}$ obtained from right ventricular myocytes were incorporated into a modified Luo-Rudy action potential model. Despite the higher $I_{Ca\text{-}L}$ current density utilized for female base myocytes, no differences were observed in control AP simulations for male or female base myocytes at either a slow pacing rate (Figure 10A) or a rapid pacing rate (Figure 10B). To mimic LQT2, a 50% reduction in I_{Kr} amplitude was then applied to the model. This partial block of I_{Kr} resulted in a small prolongation of the simulated action potentials observed in

male base cells, at both slow and fast pacing rates, as well as in female base cells with rapid pacing. However, the 50% I_{Kr} block and slow pacing rate resulted in the firing of EADs in the female base myocyte model (Figure 10A). The higher $I_{Ca\text{-}L}$ density in the female base cells allows the cell to remain in the depolarized state longer, thus causing an increase in action potential duration. The prolonged action potential durations also allow the L-type calcium channel to reactivate, thereby producing the EADs.

A)

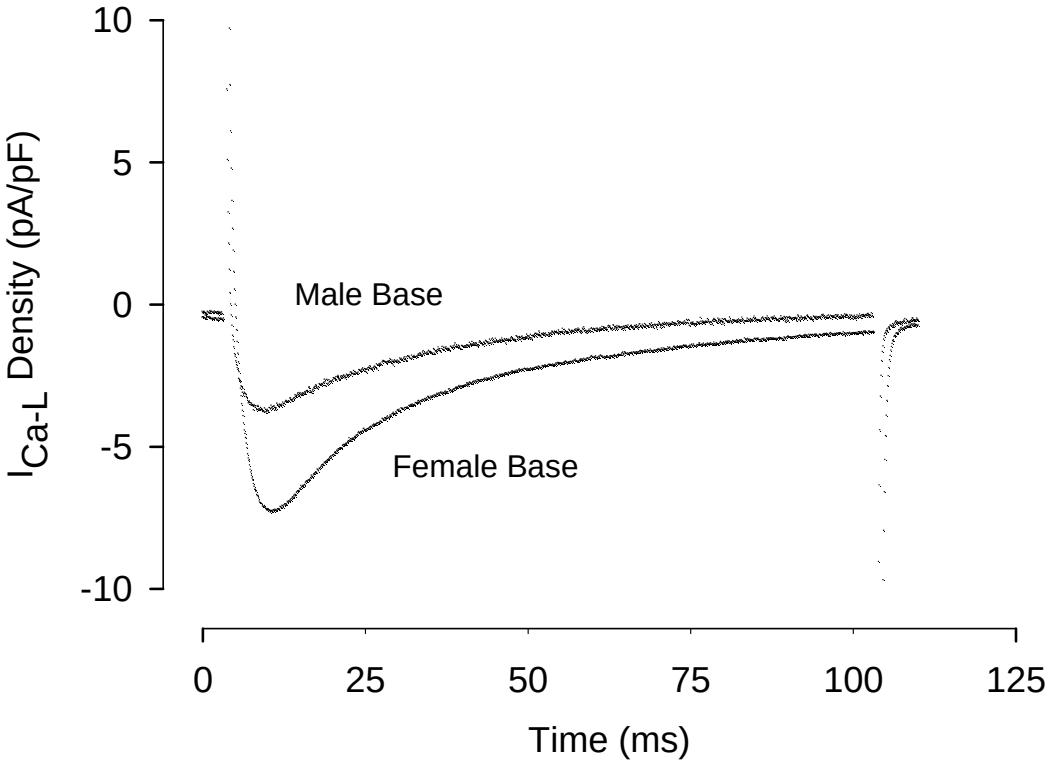
10
5
0
-5
-10
$I_{Ca\text{-}L}$ Density (pA/pF)
Male Base
Female Base
0
25
50
75
100
125
Time (ms)

B)

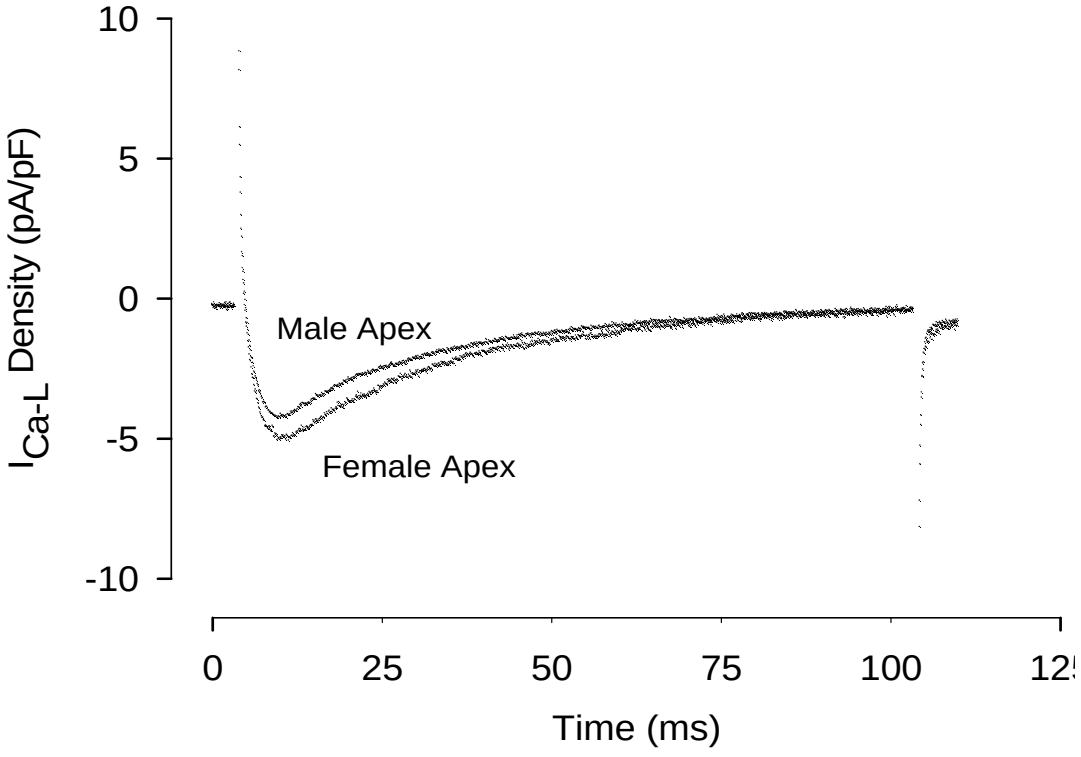
10
5
0
-5
-10
$I_{Ca\text{-}L}$ Density (pA/pF)
Male Apex
Female Apex
0
25
50
75
100
Time (ms)

Figure 4: Representative Current Tracings of $I_{Ca\text{-}L}$ Sex Differences – Current tracings of $I_{Ca\text{-}L}$ obtained at 0 mV. **A)** Whole cell calcium current densities obtained from female base region myocytes (n=8) showed consistently larger peak amplitudes than currents observed in male base myocytes (n=12). **B)** Calcium currents from male (n=4) and female (n=9) apex myocytes show little difference in peak amplitude.

A)

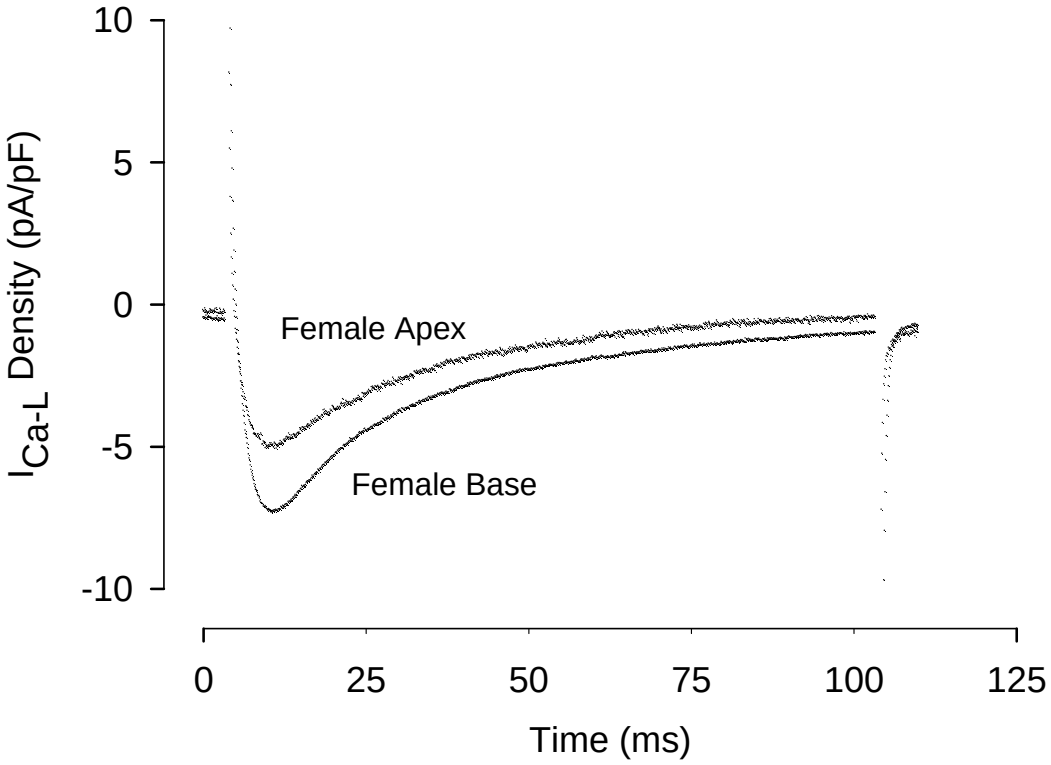
10
5
0
-5
-10
$I_{Ca\text{-}L}$ Density (pA/pF)
Female Apex
Female Base
0
25
50
75
100
125
Time (ms)

B)

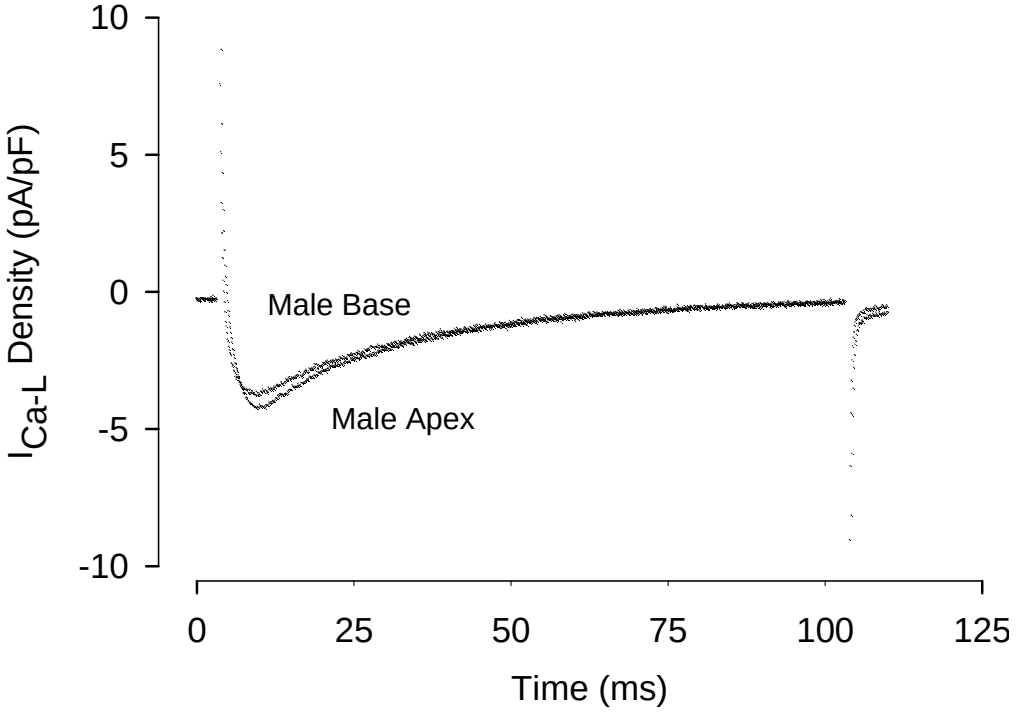
10
5
0
-5
-10
$I_{Ca\text{-}L}$ Density (pA/pF)
Male Base
Male Apex
0
25
50
75
100
125
Time (ms)

Figure 5: Representative Current Tracings of $I_{Ca\text{-}L}$ Regional Differences - Current tracings of $I_{Ca\text{-}L}$ obtained at 0 mV. **A)** Whole cell calcium current densities obtained from female base region myocytes (n=8) showed consistently larger peak amplitudes than currents observed in female apex myocytes (n=9). **B)** Calcium currents from male apex (n=4) and base (n=12) myocytes show little difference in peak amplitude.

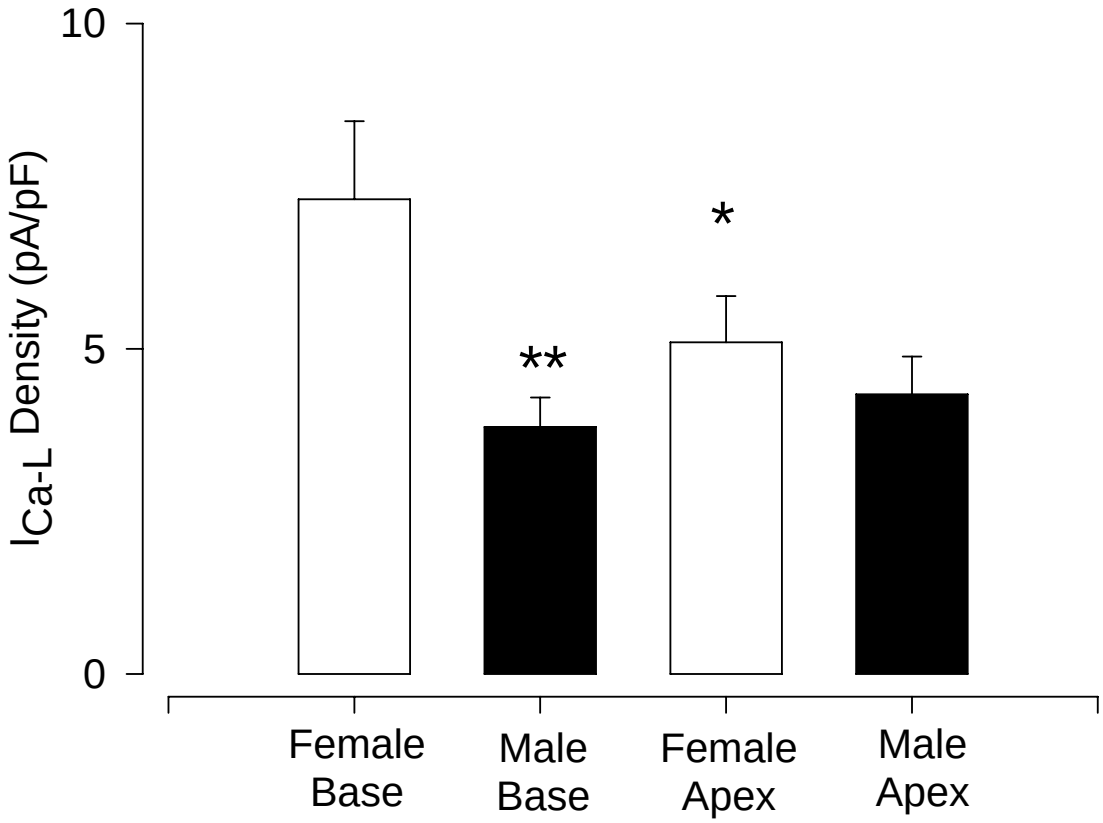
10
5
0
$I_{Ca\text{-}L}$ Density (pA/pF)
**
*
Female Base
Male Base
Female Apex
Male Apex

Figure 6: Cumulative Data – Summary of the sex and regional differences found in the peak $I_{Ca\text{-}L}$ density of adult male and female right ventricle myocytes. $I_{Ca\text{-}L}$ density was 84.6% higher in female base myocytes (7.2±0.83 pA/pF, n=8) compared to male base myocytes (3.9±0.38, n=12, $p<0.001$). Analysis of regional differences in $I_{Ca\text{-}L}$ revealed a 56.5% higher current density in female base myocytes (7.2±0.83 pA/pF, n=8) compared to female apex myocytes (4.6±0.45 pA/pF, n=9, $p<0.02$). There were no significant differences in $I_{Ca\text{-}L}$ density between female or male apex myocytes or between male apex and male base myocytes. (** = $p<0.001$; * = $p<0.02$)

A)

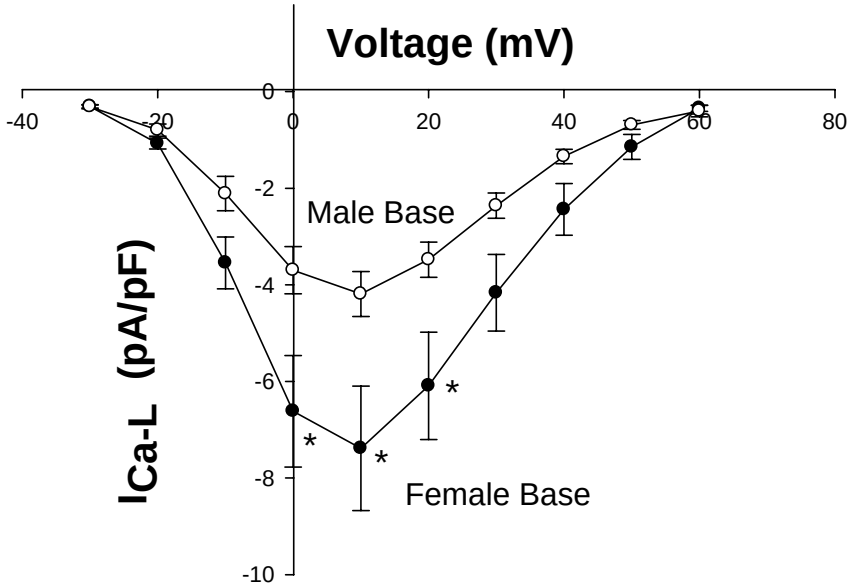
Voltage (mV)
0
-40
-20
0
20
40
60
80
-2
-4
-6
-8
-10
Male Base
Female Base
*
*
*
$I_{Ca\text{-}L}$ (pA/pF)

B)

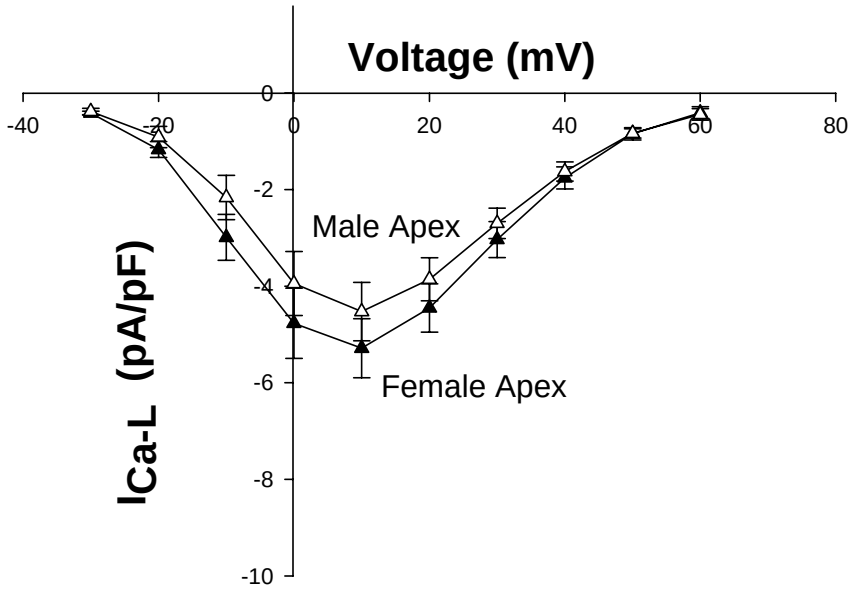
Voltage (mV)
0
-40
-20
0
20
40
60
80
-2
-4
-6
-8
-10
Male Apex
Female Apex
$I_{Ca\text{-}L}$ (pA/pF)

Figure 7: IV Relationships, Sex Differences – Current –voltage relationships for the peak $I_{Ca\text{-}L}$ density were obtained from myocytes by stepping from a holding potential of -80 mV to step potentials of -30 to +60 mV. **A)** Maximum $I_{Ca\text{-}L}$ peak current densities were significantly larger in female base myocytes (n=6) (filled circles) compared to male base myocytes (n=8) (open circles) (* = $p<0.05$). **B)** Peak current densities for $I_{Ca\text{-}L}$ in male (n=4) and female (n=7) apex myocytes were similar over all voltages examined.

A)

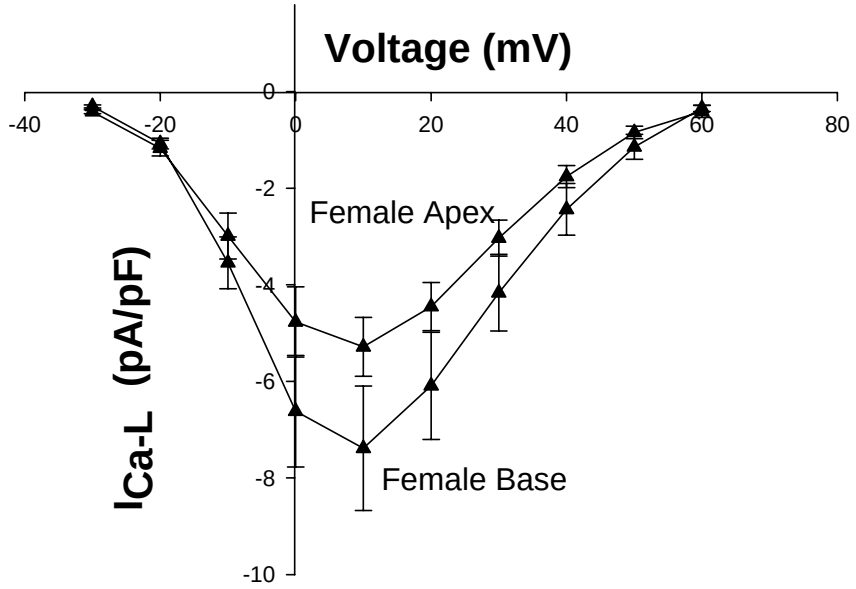
Voltage (mV)
0
-40
-20
0
20
40
60
80
-2
-4
-6
-8
-10
Female Apex
Female Base
ICa-L (pA/pF)

B)

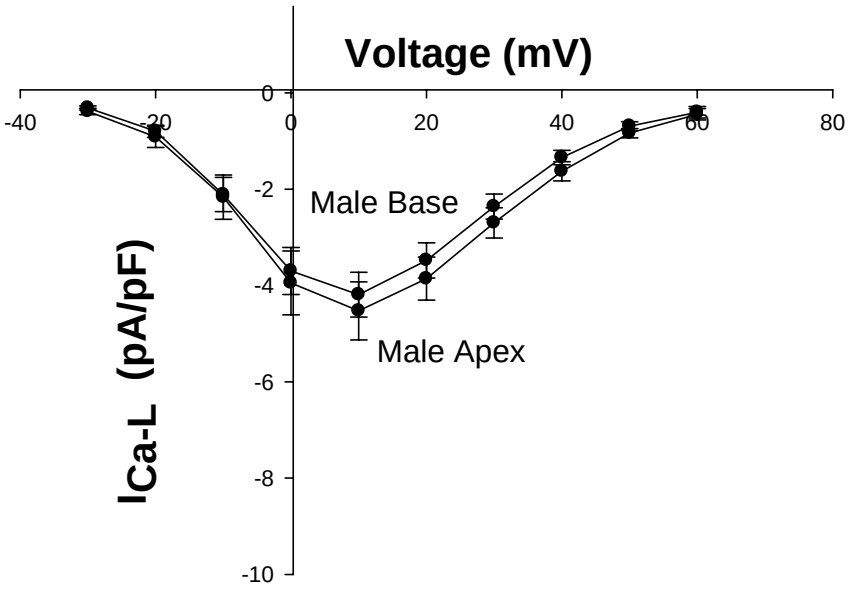
Voltage (mV)
0
-40
-20
0
20
40
60
80
-2
-4
-6
-8
-10
Male Base
Male Apex
ICa-L (pA/pF)

Figure 8: IV Relationships, Regional Differences – Current –voltage relationships for the peak $I_{Ca\text{-}L}$ density were obtained from myocytes by stepping from a holding potential of -80 mV to step potentials of -30 to +60 mV. **A)** Peak current densities for $I_{Ca\text{-}L}$ in female apex (n=7) and base (n=6) myocytes were similar over all voltages examined. **B)** Peak current densities for $I_{Ca\text{-}L}$ in male apex (n=4) and base (n=8) myocytes were similar over all voltages examined.

A)

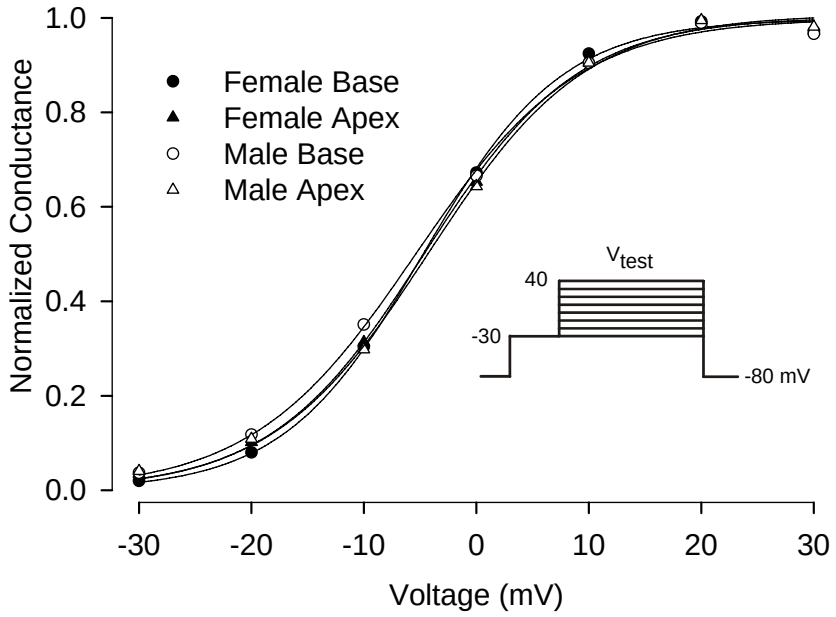
Normalized Conductance
1.0
0.8
0.6
0.4
0.2
0.0
Female Base
Female Apex
Male Base
Male Apex
V_{test}
40
-30
-80 mV
-30
-20
-10
0
10
20
30
Voltage (mV)

B)

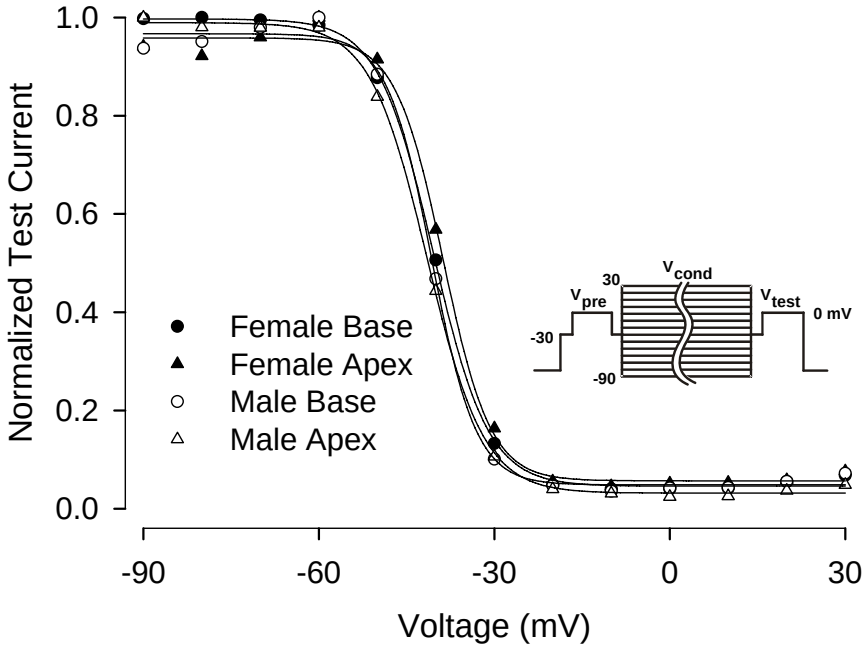
Normalized Test Current
1.0
0.8
0.6
0.4
0.2
0.0
Female Base
Female Apex
Male Base
Male Apex
V_{cond}
30
V_{pre}
V_{test}
0 mV
-30
-90
-90
-60
-30
0
30
Voltage (mV)

Figure 9: Biophysical Properties - Voltage dependence of $I_{Ca\text{-}L}$ activation and inactivation in male and female adult rabbit right ventricle apex and base myocytes. Insets show diagrams of voltage protocols used to generate experimental data.
A) Calcium current activation curves from male and female right ventricle apex and base myocytes constructed by plotting normalized conductance as a function of test potential.
B) Steady state $I_{Ca\text{-}L}$ inactivation curves from male and female apex and base right ventricle myocytes.

	Activation				Inactivation		
	V_r (mV)	$V_{0.5}$ (mV)	Slope	n	$V_{0.5,inact}$ (mV)	Slope	n
Male							
Apex	54.5 ± 0.3	-4.8 ± 1.2	6.9 ± 0.2	4	-38.8	-4.1	1
Base	52.3 ± 0.4	-4.3 ± 1.1	6.6 ± 0.1	8	-40.4 ± 0.2	-4.7 ± 0.1	4
Female							
Apex	52.8 ± 1.1	-5.1 ± 1.8	6.6 ± 0.2	7	-40.1 ± 0.6	-3.8 ± 0.1	4
Base	52.7 ± 0.7	-4.8 ± 0.4	6.3 ± 0.2	6	-41.5 ± 0.1	-4.9 ± 0.1	2

Table 2: Activation and Inactivation Parameters - Parameters of voltage-dependent $I_{Ca\text{-}L}$ activation and inactivation in adult rabbit right ventricle apex and base myocytes. The parameters for the voltage dependence of activation were obtained from the least squares fit of data points to the equation: $g/g_{max} = 1/(1 + \exp -((V_T – V_{0.5})/b))$, where g/g_{max} represents the normalized Ca^{2+} conductance, V_T represents test potentials from -30 to 30 mV, $V_{0.5}$ is the potential at which activation was half maximal, and b is the slope. The conductance at each test potential was calculated using the reversal potential (V_r) obtained from the current voltage relationship measured under each set of conditions. Parameters for the voltage dependence of inactivation were obtained from the equation: $I = I_{ir} + (1 - I_{ir})/(1 + \exp -((V_c - V_{0.5})/b))$, where I is the normalized magnitude of the peak inward current measured during a test pulse to 0 mV following a 5 sec conditioning pulse (V_c) to membrane potentials between -50 and 20 mV, I_{ir} is the inactivation resistant current, $V_{0.5}$ is the potential at which inactivation was half maximal, and b is the slope. The current elicited during the test pulse was normalized to the magnitude of the current recorded during a pretest pulse to 0 mV, which preceded each conditioning pulse.

A)

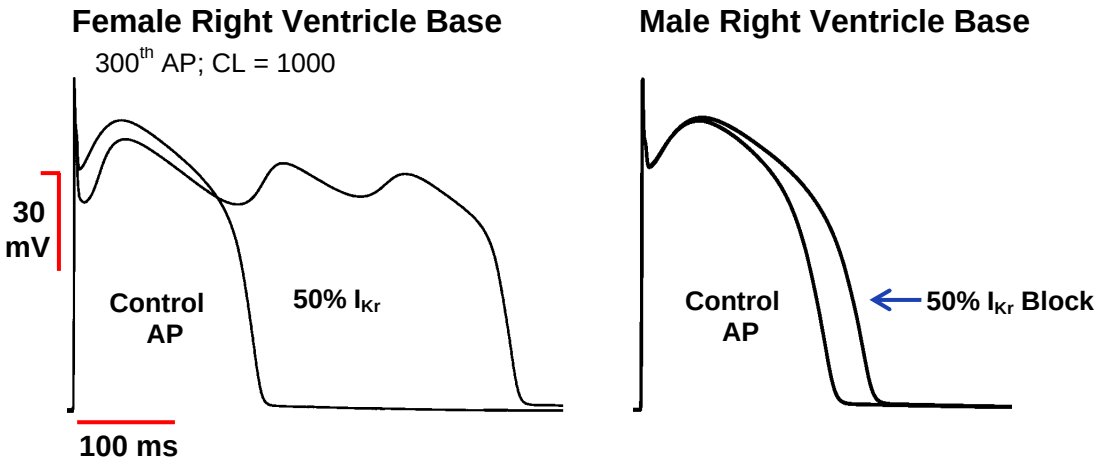
Female Right Ventricle Base
300th AP; CL = 1000
30 mV
Control AP
50% IKr
100 ms
Male Right Ventricle Base
Control AP
50% IKr Block

B)

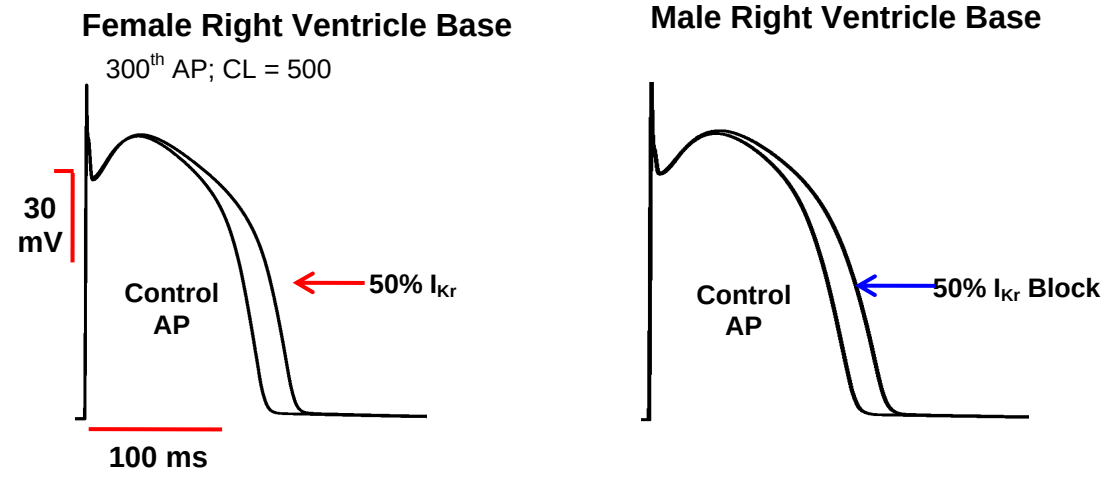
Female Right Ventricle Base
300th AP; CL = 500
30 mV
Control AP
50% IKr
100 ms
Male Right Ventricle Base
Control AP
50% IKr Block

Figure 10: Luo-Rudy Action Potential Model – Examples of cardiac action potential simulation produces by the Luo-Rudy AP model using experimentally determined sex differences in $I_{Ca\text{-}L}$ densities in female and male base myocytes. A 50% block of I_{Kr} was utilized to mimic LQT2. **A)** AP simulations for male and female base myocytes. The simulated AP's represent the 300^{th} AP from a train of AP's stimulated at a slow pacing rate (Cycle length (CL) = 1000 ms.). **B)** AP simulations conducted with the same condition, but at a faster pacing rate (CL = 500 ms.).

CHAPTER 4

IV. Discussion

This study observed sex and regional differences of $I_{Ca\text{-}L}$ in the adult rabbit cardiac myocyte. The main findings of the study show significant sex and regional differences in the peak $I_{Ca\text{-}L}$ density in the right ventricle of adult rabbits. Adult female rabbits exhibited a significantly larger peak $I_{Ca\text{-}L}$ density, almost a two-fold increase, in the base region of the right ventricle when compared to the base region of age-matched males. Female rabbits also exhibited significantly larger peak $I_{Ca\text{-}L}$ density in the base region when compared to the female apex. No significant sex differences in $I_{Ca\text{-}L}$ density in the apex region were observed, nor were any regional differences seen in the male myocytes. A previous study has reported similar sex and regional differences in $I_{Ca\text{-}L}$ in the left ventricle of adult rabbits (Sims et al. 2008). Adult female rabbits exhibited a significantly larger peak $I_{Ca\text{-}L}$ in the base region of the left ventricle when compared to the adult male base region. Adult female rabbits also exhibited significantly larger peak $I_{Ca\text{-}L}$ in the base region of the left ventricle when compared to the apex of the left ventricle. This study, combined with the results presented here, suggest that elevated $I_{Ca\text{-}L}$ density may play an important role in the genesis of cardiac arrhythmias.

Activation and inactivation properties of the $I_{Ca\text{-}L}$ were also examined in right ventricular myocytes. Any differences in the activation or inactivation properties of $I_{Ca\text{-}L}$ in female base cells would indicate that some other factors, such as an increase in channel opening duration, could be responsible for the increase in peak $I_{Ca\text{-}L}$. However, there were no differences found in activation or inactivation properties between the four examined regions.

Experimental findings were used to generate a modified Luo-Rudy action potential model. In this model, I_{Kr} was blocked by 50% in order to mimic LQT2 and observe whether EADs would occur in any of the four myocyte regions. EAD genesis in any region other than female base would lead us to conclude that the increase in $I_{Ca\text{-}L}$ is not responsible for the generation of the EADs. However, EADs were only observed in the female base region when stimulated at a slower pacing rate. The increase of $I_{Ca\text{-}L}$ in female base regions allows the cell to remain in the depolarized state for a longer time, thereby causing an increase in action potential duration. This increased duration contributes to the reactivation of the L-type calcium channel, resulting in the production of EADs. Sims et al. (2008), experimentally examined action potential durations and the propensity of EADs to be elicited under varied conditions. EAD genesis was found only in the adult female left ventricular base cells under 50% I_{Kr} block, mimicking LQT2.

Sims et al. (2008), also studied sex and regional differences of $I_{Ca\text{-}L}$ in the left ventricle of pre-pubertal rabbits. If significant differences in $I_{Ca\text{-}L}$ density in different myocytes was not seen in pre-pubertal rabbits, then this suggests that the observed differences in peak $I_{Ca\text{-}L}$ in adult rabbits is due to hormonal regulation following puberty. However, pre-pubertal male rabbits exhibited larger peak $I_{Ca\text{-}L}$ in the base of the left ventricle when compared to age matched females. Pre-pubertal males also exhibited larger peak $I_{Ca\text{-}L}$ in the base region of the left ventricle when compared to apex. This allows us to determine that the difference in arrhythmia vulnerability can not be primarily due to changes in post-pubertal sex hormone levels as previously thought.

This is an important study due to the high incidence of cardiac disease and sudden death related to arrhythmias. The right ventricle is responsible for sending deoxygenated

blood to the lungs, where exchange of oxygen and carbon dioxide can occur. There are many heart diseases that result from the right ventricle not functioning properly, such as acute right ventricle myocardial infarction and chronic right ventricle failure. One of the most well-known right ventricle diseases is arrhythmogenic right ventricular cardiomyopathy (Basso et al. 2009). This is an inherited heart muscle disorder which causes damaged heart muscle to gradually be replaced by scar tissue and fat and can cause sudden death in young people due to the altered electrical rhythm of the heart (Basso et al. 2009).

There were some limitations to the findings reported in this study. First, we were unable to obtain recordings from a sufficient number of male apex myocytes to allow us to conclude that there were no differences between male apex myocytes and the other three regions in the activation and inactivation properties of the L-type calcium channel. Second, although the L-type Ca^{2+} channel predominates in cardiac myocytes, other channel types may also be responsible for regulating calcium entry into the cell. Without examining each channel and its role, we are unable to definitively state that $I_{Ca\text{-}L}$ is the only factor responsible for the observed increase in current density at the female base region.

Hormonal regulation of $I_{Ca\text{-}L}$ must be completely understood to improve the understanding of our study. The mechanism responsible for testosterone acting on the signaling of potassium channels is not yet fully understood. It is thought that testosterone up regulates the potassium channels allowing the repolarization of the cardiac action potential to occur faster (Pham et al. 2001). This would explain why men have a decreased risk of experiencing EADs due to reactivation of the L-type calcium current.

However, pre-pubertal male rabbits were found to exhibit higher peak $I_{Ca\text{-}L}$ and an increased risk for developing EADs under conditions mimicking LQT2 (Sims et al. 2008). This shows that there must be factors other than hormonal regulation that are responsible for the differences of peak $I_{Ca\text{-}L}$ density in pre-pubertal male rabbits and adult female rabbits. There is also evidence that progesterone and estrogen are factors in regulating $I_{Ca\text{-}L}$ levels (Nakamura et al. 2007).

There are many future directions to take with this study. Western blotting can be performed in order to determine whether the increase in peak $I_{Ca\text{-}L}$ density is in fact an increase in the number of calcium channels and not due to altered regulation of those channels. The effect of beta-adrenergic regulation on the channels must also be studied. Most LQT2 arrhythmias occur during emotional distress, which is linked to activation of the beta-adrenergic pathway (Moss et al. 2005). In addition, this study only theoretically examined whether the increased $I_{Ca\text{-}L}$ exhibited by the female base regions would produce EADs under conditions mimicking LQT2. The next step would be to experimentally treat the cells with a K^+ blocking drug, such as E4301, and examine whether EADs would in fact occur under conditions that mimic LQT2. In the model, $I_{Ca\text{-}L} = dff_{Ca}I_{Ca}$. Activation and inactivation parameters may be incorporated in the mathematical model in order to determine the modified forms of the voltage dependent steady-state activation and inactivation curves given by $d_\infty(v)$ and $f_\infty(v)$ for the activation and inactivation gating variables d and f.

In conclusion, a significant increase in $I_{Ca\text{-}L}$ density in the right ventricle of the female base region was observed. This higher current density of $I_{Ca\text{-}L}$ in the base region of right ventricule myocytes did result in the generation of EADs through the use of our

mathematical action potential model. The generation of EADs may result in the generation of an arrhythmia. However, a mechanism for arrhythmia generation has yet to be found.

IV. REFERENCES

Bai, C., Namekata, I., Kurokawa, J., Tanaka, H., Shigenobu, K., Furukawa, T. (2005). Role of nitric oxide in Ca^{2+} sensitivity of the slowly activating delayed rectifier K^+ current in cardiac myocytes. *Circ. Res.*, **96**, 64-72.

Basso, C., Corrado, D., Marcus, F., Nava, A., Thiene, G. (2009). Arrhythmogenic right ventricular cardiomyopathy. *Lancet*, **373**, 1289-1300.

Bazett, H.C. (1920). An analysis of the time relationships of the heart. *Heart*, **7**, 353-370.

Berger, F., Borchard, U., Hafner, D., Putz, I., Weiss, T.M. (1997). Effects of 17-β estradiol on action potentials and ionic currents in male rat ventricular myocytes. *Naunyn-Schmiedeberg's Arch. Pharmacol*., **356**, 788-796.

Bers, D.M. (2001a). Cardiac Action Potential and Ion Channels. In: *Excitation-Contraction Coupling and Cardiac Contractile Force.* Kluwer Academic Publishers, pp. 63-100.

Bers, D.M. (2001b). Ca Influx via Sarcolemmal Ca channels. In: *Excitation-Contraction Coupling and Cardiac Contractile Force.* Kluwer Academic Publishers, pp. 101-130.

Bodi, I., Mikala, G., Koch, S.E., Akhter, S.A., Schwartz, A. (2005). The L-type calcium channel in the heart: the beat goes on. *J. Clin. Invest*., **115**(12), 3306-3317.

Camm, A.J., Malik, M., Yap, Y.G. (2004). *Acquired long QT syndrome*. Blackwell Publishing.

Catterall, W.A. (2000). Structure and regulation of voltage-gated Ca^{2+} channels. *Ann. Rev. Cell Dev. Biol.*, **16**, 521-555.

Cheng, J, Kamiya, K, Liu, W, Tsuji, Y, Toyama, J, Kodama, I. (1999). Heterogeneous distribution of the two components of delayed rectifier K^+ currents: a potential mechanism of the proarrhythmic effects of methanesulfonanilide class III agents. *Cardiovasc. Res.*, **43**, 135-147.

Chu, S.H., Sutherland, K., Beck, J., Kowalski, J., Goldspink, P., Schwertz, D. (2005). Sex differences in expression of calcium-handling proteins and beta-adrenergic receptors in rat heart ventricle. *Life Sci.,* **76**, 2735-2749.

Curran, M.E., Splawski, I., Timothy, K.W., Vincent, G.M., Green, E.D., Keating, M.T. (1995). A molecular basis for cardiac arrhythmias: HERG mutations cause long QT syndrome. *Cell*, **80**, 795-803.

Ding, S., Kuroki, S., Kameyama, A., Yoshimura, A. & Kameyama, M. (1999). Cloning and expression of the Ca^{2+} channel α_{1C} and β_{2a} subunits from guinea pig heart. *J. Biochem. (Tokyo)*, **125**, 750-759.

Dumaine, R., Towbin, J.A., Brugada, P., Vatta, M., Nesterenko, D.V., Nesterenko, V.V., Brugada, J., Brugada, R., Antzelevich, C., (1999). Ionic mechanism responsible for the electrocardiographic phenotype of the brugada syndrome are temperature dependent. *Circ. Res.,* **85**, 803-809.

Ebert, S.N., Liu, X., Woosley, R. (1998). Female gender as a risk factor for drug-induced cardiac arrhythmias: Evaluation of Clinical and Experimental Ecidence. *J. Women's Health*, **7**(5), 547-557.

Faber, G.M., Rudy, Y. (2000). Action potentials and contractility changes in [Na+]I overload cardiac myocytes: a stimulation study. *Biophys. J.*, **78**, 2392-2404.

Gupte, S.A., Tateyama, M., Okada, T., Oka, M., Ochi, R. (2002). Epiandrosterone, a metabolite of testosterone precursor, blocks L-type calcium channels of ventricular myocytes and inhibits myocardial contractility. *J. Mol. Cell Cardiol.,* **34**, 679-688.

Gurnett, C.A., De Ward, M. & Campbell, K.P. (1996). Dual function of the voltage-dependent Ca^{2+} channel α_2 δ subunit in current stimulation and subunit interaction. *Neuron*, **16**, 431-440.

Gyorke, S., Terentyev, D. (2008). Modulation of ryanodine receptor by luminal calcium and accessory proteins in health and cardiac disease. *Cardiovasc. Res*., **77**, 245-255.

Hamill, O.P., Marty, A., Neher, E., Sakmann, B., Sigworth, F.J. (1981). Improved patch-clamp techniques for high-resolution current recording from cells and cell-free membrane patches. *Pfugers Arch.*, **391**, 85-100.

Hedley, P.L., Jergensen, P., Schlamowitz, S., Wangari, R., Moolman-Smook, J., Brink, P.A., Kanters, J.K., Corfield, V.A., Christiansen, M. (2009). The genetic basis of long QT and short QT syndromes: A Mutation Update. *Human Mutation*, **30**(11), 1486-1511.

January, C.T., Riddle, J.M. (1989). Early Afterdepolarizations: mechanism of induction and block. A role for L-Type Ca^{2+} current. *Circ. Res.*, **64**(5), 977-990.

Jay, S.D., Sharp, A.H., Kahl, S.D., Vedvick, T.S., Harpold, M.M. & Campbell, K.P. (1991). Structural characterization of the dihydropyridine-sensitive calcium channel α_2-subunit and the associated δ peptides. *J. Biol. Chem.*, **266**, 3287-3293.

Keef, K.D., Hume, J.R. & Zhong, J. (2001). Regulation of cardiac and smooth muscle Ca^{2+} channels (Ca(V)1.2a,b) by protein kinases. *Am. J. Physiol Cell Physiol.*, **281**, C1743-C1756.

Lehmann, M.H., Haray, S., Archibald, D., Quart, B., MacNeil, D.J. (1996). Sex differences in risk of Torsade de pointes with d,1-sotalol. *Circulation*, **94**, 2535-2541.

Liu, T, Choi, B.R., Salama, G. (2005). Sex modulates the arrhythmogenic substrate in prepubertal rabbit hearts along with Long QT2. *J. Cardiovasc. Electrophys*., **16(5)**, 516-524.

Merri, M, Benhorin, J, Alberti, M, Locati, E, Moss, A.J. (1989). Electrocardiographic quantitation of ventricular repolarization. *Circulation*, **80**(5), 1301-8.

Moss, A., Kass, R.S. (2005). Long QT syndrome: from channels to cardiac arrhythmias. *J. Clin. Invest.*, **115**(8), 2018-2024.

Mukherjee, R., Hewett, K.W., Walker, J.D., Basler, C.G., Spinale, F.G. (1998). Changes in L-type calcium channel abundance and function during the transition to pacing-induced congestive heart failure. *Cardiovasc. Res*., **37**, 432-444.

Nakajima, T., Iwasawa, K., Oonuma, H., Morita, T., Goto, A., Wang, Y., Hazama, H. (1999). Antiarrhythmic effect and its underlying ionic mechanism of 17 β–estradiol in cardiac myocytes. *Br. J. Pharmacol*., **127**, 429-440.

Nakamura, H., Kurokawa, J., Bai, C., Asada, K., Xu, J., Ronit, V.O., Zhu, Z.I., Clancy, C.E., Isobe, M., Furukawa, T. (2007). Progesterone regulates cardiac repolarization through a nongenomic pathway: an in vitro patch-clamp and computational modeling study. *Circulation*, **116**, 2918-2922.

Patterson, E., Lazzara, R., Szabo, B., Liu, H., Tang, D., Li, Y., Scherlag, B.J., Po, S.S. (2006). Sodium-calcium exchange initiated by the Ca^{2+} transient: an arrhythmia trigger within pulmonary veins. *J. Am. Coll. Cardiol*., **47**(6), 1196-1206.

Perez-Reyes, E., Cribbs, L.L., Daud, A., Lacerda, A.E., Barclay, J., Williamson, M.P., Fox, M., Rees, M., Lee, J. (1998). Molecular characterization of a neuronal low-voltage-activated T-type calcium channel. *Nature*, **391**, 896-900.

Pham, T. V., E. A.Sosunov, Gainullin, R.Z., Danilo, P., Rosen, M.R. (2001). Impact of sex and gonadal steroids on prolongation of ventricular repolarization and arrhythmias induced by I(K)-blocking drugs. *Circulation*, **103**(17), 2207-12.

Pham, T. V., Robinson, R.B., Danilo, P., Rosen, M.R. (2002). Effects of gonadal steroids on gender-related differences in transmural dispersion of L-type calcium current. *Cardiovasc. Res.,* **53**(3), 752-62.

Pham, T. V., Rosen, M.R. (2002). Sex, hormones, and repolarization. *Cardiovasc Res,* **53**(3), 740-51.

Schwarts, P.J., Wolf, S. (1978). QT interval prolongation as predictor of sudden death in patients with myocardial infarction. *Circulation*, **57**, 1074-1077.

Sims, C., Harvey, R.D. (2004). Redox modulation of basal and beta-adrenergically stimulated cardiac L-type Ca2+ channel activity by phenylarsine oxide. *Br. J. Pharmacol.*, **142**(4), 797-807.

Sims, C., Reisenweber, S., Viswanathan, P.C., Choi, B.R., Walker, W.H., Salama, G. (2008). Sex, age, and regional differences in L-type calcium current are important determinants of arrhythmia phenotype in rabbit hearts with drug-induced long QT type 2. *Circ. Res.,* **102**(9), 86-100.

Vincent, G.M. (2002). The long QT syndome. *Indian Pacing Electrophysiol. J.*, **2**(4), 127-142.

Northeastern Ohio Universities Colleges of Medicine and Pharmacy

TO: Carl Sims, Ph.D.
Assistant Professor, Biological Sciences
Youngstown State University

FROM: Hans G. Folkesson, Ph.D.
Chairperson, NEOUCOM/P Institutional Animal
Care and Use Committee

SUBJECT: Protocol Approval

DATE: July 31, 2008

The following Northeastern Ohio Universities Colleges of Medicine and Pharmacy (NEOUCOM/P) animal use protocol was reviewed and approved by this Institution's Animal Care and Use Committee (IACUC) on July 31, 2008. The protocol is approved for a three (3) year period of time; however you must submit an annual renewal to the IACUC each year for review.

Any serious or adverse events regarding the use of animals approved in this study must be reported immediately to the IACUC Chairperson or the Attending Veterinarian. Protocols involving the use of human tissues require Institutional Review Board (IRB) approval.

NEOUCOM/COP Protocol No.:	**#08-021**
Title of Protocol:	**Cardiac Dynamics and Susceptibility to Rhythm Disturbances**
Type of Vertebrate:	**Rabbits**
Funding Agency:	**National Science Foundation**
Protocol Expiration Date:	**July 30, 2011**

This institution has an Animal Welfare Assurance on file with the Office of Laboratory Animal Welfare (OLAW). The Assurance number is A3474-01. This institution is also registered with the United States Department of Agriculture (USDA). The USDA registration number is 31-R-0092.

The Comparative Medicine Unit (CMU) at the Northeastern Ohio Universities Colleges of Medicine and Pharmacy (NEOUCOM/P) has been accredited with the Association for Assessment for Accreditation of Laboratory Animal Care (AAALAC) International since June 8, 1982. Full accreditation was last renewed on June 26, 2008.

Thank you.

HGF:lkn

Cc: Walter E. Horton, Jr., Ph.D.
Vice President for Research
NEOUCOM/P Institutional Official

File